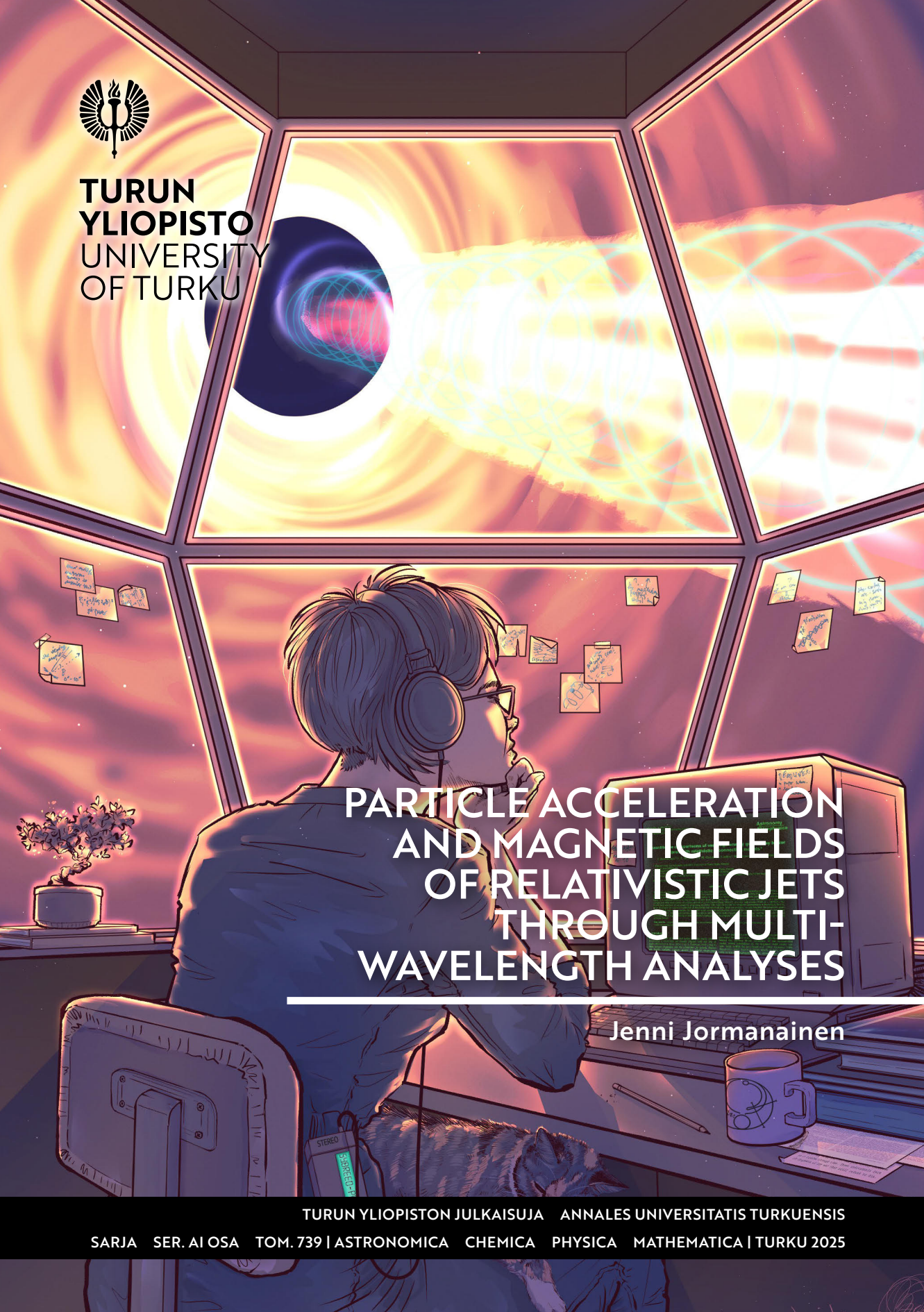

TURUN YLIOPISTO
UNIVERSITY OF TURKU

PARTICLE ACCELERATION AND MAGNETIC FIELDS OF RELATIVISTIC JETS THROUGH MULTI-WAVELENGTH ANALYSES

Jenni Jormanainen

TURUN YLIOPISTON JULKAISUJA ANNALES UNIVERSITATIS TURKUENSIS
SARJA SER. AI OSA TOM. 739 | ASTRONOMICA CHEMICA PHYSICA MATHEMATICA | TURKU 2025

TURUN
YLIOPISTO
UNIVERSITY
OF TURKU

PARTICLE ACCELERATION AND MAGNETIC FIELDS OF RELATIVISTIC JETS THROUGH MULTI-WAVELENGTH ANALYSES

Jenni Jormanainen

TURUN YLIOPISTON JULKAISUJA ANNALES UNIVERSITATIS TURKUENSIS
SARJA SER. AI OSA TOM. 739 | ASTRONOMICA CHEMICA PHYSICA MATHEMATICA | TURKU 2025

University of Turku

Faculty of Science
Department of Physics and Astronomy
Astronomy
Doctoral programme in Exact Sciences

Supervised by

Docent Talvikki Hovatta
Finnish Centre for Astronomy with ESO
University of Turku, Finland;
Aalto University Metsähovi Radio
Observatory, Finland

Docent Elina Lindfors
Department of Physics and Astronomy
University of Turku, Finland

Reviewed by

Associate Professor Joonas Nättilä
Department of Physics
University of Helsinki, Finland

Associate Professor Eileen Meyer
Department of Physics
University of Maryland, USA

Opponent

Associate Professor Foteini Oikonomou
Department of Physics
Norwegian University of Science and Technology
Norway

Cover Image: Drawn by Jenni Jormanainen

ISBN 978-952-02-0197-5 (PRINT)
ISBN 978-952-02-0198-2 (PDF)
ISSN 0082-7002 (PRINT)
ISSN 2343-3175 (ONLINE)
Painosalama, Turku, Finland, 2025

Iskälle

UNIVERSITY OF TURKU
Faculty of Science
Department of Physics and Astronomy
Astronomy
JORMANAINEN, JENNI: Particle Acceleration and Magnetic Fields of Relativistic Jets Through Multi-Wavelength Analyses
Doctoral dissertation, 127 pp.
Doctoral programme in Exact Sciences
May 2025

ABSTRACT

Relativistic jets launched by supermassive black holes (SMBH) are some of the most extreme phenomena in the Universe. They are best observed in blazars, where the jet is pointing almost directly towards us. This unique alignment means that the jet dominates their observed emission, making them excellent sources for studying the jet properties.

This thesis focusses on understanding the particle acceleration in blazar jets and how it is tied to their magnetic fields. Multi-wavelength (MWL) data from four blazars are analysed using various methods. Particle acceleration mechanisms are also explored through magnetic reconnection simulations in the case of one source.

Brightness variations of blazars can be observed across the entire electromagnetic spectrum on timescales of years down to minutes. In the past, shocks have been shown to describe blazar flaring well, and the MWL polarisation data analysed from one blazar (Mrk 501) as part of this thesis supports this scenario. At the same time, minute-scale flares in the very high-energy (VHE, $E > 100$ GeV) gamma rays are difficult to explain with shocks. Magnetic reconnection from a small region could provide a solution to this. Magnetic reconnection simulations are tested in the case of Mrk 421, and they are found to reproduce the observed VHE flaring.

The co-existence of two different acceleration mechanisms can be possible if there are several emitting regions within the jet. The broad-band spectrum of one source (VER J0521+211) is modelled, and the high energy emission is found to originate from a smaller region closer to the SMBH where also magnetic reconnection could take place. In the same study, modelling of the long-term optical polarisation supports the need for several components to produce the observed polarisation.

An analysis of MWL polarisation observation together with very long baseline interferometry data is used to track a moving jet component passing through a stationary shocked region of the jet of OJ 287. The passage also coincides with a VHE flare, hinting at their connection. The studies included in this thesis provide important clues for solving the open questions related to particle acceleration and the magnetic fields in blazar jets.

KEYWORDS: active galactic nuclei, relativistic jets, blazars, magnetic fields, particle acceleration

TURUN YLIOPISTO
Matemaattis-luonnontieteellinen tiedekunta
Fysiikan ja tähtitieteen laitos
Tähtitiede
JORMANAINEN, JENNI: Particle Acceleration and Magnetic Fields of Relativistic Jets Through Multi-Wavelength Analyses
Väitöskirja, 127 s.
Eksaktien tieteiden tohtoriohjelma
Toukokuu 2025

TIIVISTELMÄ

Supermassiivisten mustien aukkojen syöksemät relativistiset hiukkassuihkut ovat eräitä maailmankaikkeutemme energisimmistä ilmiöistä. Blasaareissa toinen suihkuista osoittaa lähes suoraan meitä kohti. Tämän katselukulman vuoksi suihku hallitsee blasaareista havaittavaa säteilyä tehden niistä oivia kohteita suihkujen tutkimiseen.

Tässä väitöskirjassa tutkitaan hiukkaskiihdytystä sekä sen yhteyttä blasaarisuihkujen magneettikenttiin analysoimalla havaintoja usealta aallonpituudelta neljästä eri blasaarista. Lisäksi hiukkaskiihdytystä tutkitaan analysoimalla magneettisen rekonnektion simulaatioita yhdelle kohteelle.

Blasaarien kirkkausvaihtelua voidaan havaita kaikilla aallonpituuksilla. Purkauksien aikaskaalat vaihtelevat vuosista muutamiin minuutteihin. Aiemmat tutkimukset ovat osoittaneet, että hitaampia purkauksia voidaan mallintaa tarkoin shokkiaalloilla. Tässä väitöskirjassa usealla aallonpituudella tehdyt polarisaatiohavainnot blasaarista Mrk 501 tukevat shokkimallien ennustuksia. Toisaalta erittäin korkeaenergisen gammasäteilyn alueella nähtäviä minuuttiaikaskaalan purkauksia nämä mallit eivät kuvaa yhtä hyvin. Pienellä emissioalueella tapahtuva magneettinen rekonnektio voisi ratkaista tämän ongelman. Tässä väitöskirjassa erään rekonnektiomallin osoitetaan tuottavan blasaarin Mrk 421:n purkauksia vastaavia tuloksia.

Useampi hiukkaskiihdytysmekanismi voisi vaikuttaa blasaarisuihkuissa, jos ne toimisivat eri alueilla. Blasaarin VER J0521+211:n monitaajuussäteilyä mallintamalla huomataan, että korkeaenerginen säteily on peräisin pienemmältä alueelta mustan aukon läheisyydestä. Myös rekonnektiota voisi tapahtua tuolla alueella. Samassa tutkimuksessa tehty optisen polarisaation mallinnus tukee tarvetta useammalle emissioalueelle.

Lopuksi väitöskirjassa tutkitaan OJ 287:n polarisaatiota sekä pitkäkantainterferometrialla tehtyjä havaintoja. Dataa analysoimalla voitiin seurata plasman liikkumista shokkialueen halki blasaarisuihkussa. Plasmatihentymän kulku shokkialueen läpi vaikuttaa myös olevan yhteydessä kirkastumiseen gamma-alueella. Tässä väitöskirjassa tehdyt tutkimukset antavat tärkeää lisätietoa hiukkaskiihdytyksestä ja magneettikentistä blasaarien hiukkassuihkuissa.

ASIASANAT: aktiivinen galaksinydin, relativistiset suihkut, blasaarit, magneettikentät, hiukkaskiihdytys

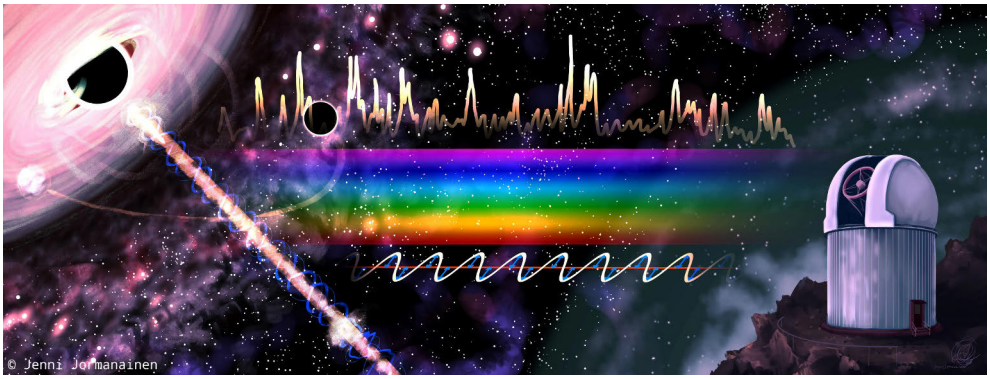

Acknowledgements

Read me about the black hole again. I look at the worn pages of a familiar book in awe and I hear it again. The call of the cosmic Beast. I go out at night just to see the glimmering specs of dust that fill the sky. What are they and where? How far? Only when my breath turns into clouds do I go back inside, but I still pull the curtains aside and fall asleep gazing at the stars.

I pack my bags and prepare for the arduous journey. The next ship to the neighbouring system leaves in five minutes. The deep dark space rocks the ship in its gravitational currents. *Land ahoy!* the captain cries as a tiny blue dot finally appears from the void. *Reef the stellar sails!*

Books and papers flood my desk over the next years. The illusion of getting closer to the stars and the Beast faded quickly as the days flew past in my small study. I have come so far, but it does not make it any closer in the grand scale of the Universe. Once again, I sneak outside at night. This time I am accompanied by many more eyes, mechanical ones, as I peer into the darkness.

The day is here. The fleet that has traversed the most perilous of tides is recruiting fresh crew members. *Think ya can do it, landlubber?* I stare into the old celestial sailor's weary eyes and nod. We board the ship as its imposing sails are being raised. *That luminous heart up there is a maelstrom like no other*, the sailor lifts his bony finger.

The magnetic shields of the mighty graviton schooner bend, but they do not break. Storm is rising and the winds are picking up. The shiny nucleus spreads

across the deep horizon, and it is too bright to look at without protective goggles. I grab the ropes and hold on tight.

We finally arrive at the port of the last stable orbit. All the books and the years of studying never prepared me for this. I hear the Beast talking to me in a secret language that is different for everyone. The raging eye of the storm and the whirlwind that cuts the sky in half are now almost within my reach.

***

This thesis work would not have been possible without my supervisor Dr. Talvikki Hovatta who found me during the third year of my Bachelor's studies and has been keeping me around ever since. Thank you for introducing me to the fascinating subject of blazars and guiding me through my Master's and now my PhD. Thank you to my second supervisor Dr. Elina Lindfors for convincing me during my first astronomy course in university that this is the subject I should pursue to study, and for taking care of me while Talvikki was on maternity leave. I could not have hoped for better supervisors! I also promised to write about the extracurricular activities I participated in during my PhD, that is, tending to Talvikki's chickens and Elina's horses. These duties should be expected from all PhD students.

Starting my first summer internship at the Tuorla Observatory was a dream come true. The historical environment in the middle of the Piikkiö forest was the best place to start. Thank you Dr. Kari Nilsson and especially Dr. Vandad Fallah Ramazani for teaching me about the optical observations and their data analysis. I am honoured to have had the chance to contribute to the Tuorla Blazar Monitoring programme. My PhD journey was made a lot easier through the pandemic times by almost weekly calls with the rest of our blazar group. Thank you Dr. Yannis Liodakis and Dr. Karri Koljonen for the helpful comments on my work. Thank you also Sofia Kankkunen (especially for our texts during tough times) and Pouya Kouch without whose peer support I could not have survived the thesis process.

The first project of my thesis on magnetic reconnection was not an easy start, and I am forever grateful for all the discussions I have had with Prof. Maria Petropoulou and Dr. Ian Christie. Thank you for your time and patience with me as I have tried to understand the more theoretical side of blazar jets.

During my time in Turku, I got to know and be a part of FINCA staff. Thank you for the friendly and encouraging working environment. And of course, I miss the corridor of the weirdos in Quantum. Thank you Dr. Pekka Heinämäki for the off-topic chats that made my workdays lighter, and for giving me the chance to gain some teaching experience. Thank you Timo Kravtsov who found me lurking in the Tuorla library during my first summer internship. Sometimes I just need to be forced to be social. After moving back to Lohja and spending more time at the Metsähovi Radio Observatory, I got to know many of the staff members there. Thank you for letting

me visit. I also got to be a part of the MAGIC Collaboration, go on observation shifts on the beautiful island of La Palma, and see those magical skies from the top of the Roque de los Muchachos. Thank you for letting me be a part of a bigger group of scientists.

I am grateful for the financial support of the Kordelin Foundation during the last year of my thesis work.

I would not have made it this far in the first place without the love and support of my parents Siru and Eino Jormanainen. Letting me be me and pursue crazy dreams like this has meant the world to me. Thank you Mom for being my role model, you are the strongest woman I know. And thank you Dad for taking me to skate, to judo, and buying me a piano when I wanted those things, even if I never became a professional in any of them. You gave me the best start to life, and I know you are still following me on my journey. Thank you to my sister Juuli for loving and supporting me even through her own struggles. You are also strong! I would not have remained sane without my sweet cat Jazzi and my pony Kaapo. Animal therapy truly is the best medicine.

Thank you Mummi, Ukki, Mummo, Juha, Jesperi, and the rest of my family for taking care of me. Thank you to my best friend Susku for staying with me through thick and thin. No matter where we end up (be it as 'vernons') we will always support each other. Thank you to all my friends for the fun times we have had through the years.

Most importantly, thank you Joel for finding my heart in this chaotic Universe. You are the most inspiring and intelligent man I know, and I am forever grateful for your love and support.

Laholm, February 2025

Jenni Jormanainen

Table of contents

List of publications

This dissertation is based on the following original publications, which are referred to in the text by their Roman numerals:

I **Quantitative comparisons of very-high-energy gamma-ray blazar flares with relativistic reconnection models**,
J. Jormanainen, T. Hovatta, I. M. Christie, E. Lindfors, M. Petropoulou, and I. Liodakis, A&A, 678, A140 (2023).

II **Polarized blazar X-rays imply particle acceleration in shocks**,
I. Liodakis, A. P. Marscher, I. Agudo, A. V. Berdyugin, M. I. Bernardos, G. Bonnoli, G. A. Borman, C. Casadio, V. Casanova, E. Cavazzuti, N. Rodriguez Cavero, L. Di Gesu, N. Di Lalla, I. Donnarumma, S. R. Ehlert, M. Errando, J. Escudero, M. García-Comas, B. Agís-González, C. Husillos, *J. Jormanainen*, et al., Nature, 611, 677–681 (2022).

III **Time-dependent modelling of short-term variability in the TeV-blazar VER J0521+211 during the major flare in 2020**,
MAGIC Collaboration, ... , *J. Jormanainen*, et al., A&A, 694, A308 (2025)

IV **The polarisation behaviour of OJ 287 viewed through radio, millimetre, and optical observations between 2015 and 2017**,
J. Jormanainen, T. Hovatta, E. Lindfors, A. Berdyugin, W. Chamani, V. Fallah Ramazani, H. Jermak, S. G. Jorstad, A. Lähteenmäki, C. McCall, K. Nilsson, P. Smith, I. A. Steele, J. Tammi, M. Tornikoski, and F. Wierda, A&A, 694, A206 (2025)

Author's contribution

Paper I: The author developed the analysis methods for the comparison of the magnetic reconnection simulations with the observed light curves. The author collected the observed VHE gamma-ray light curves and the literature values used in the simulation setup, and closely worked in improving the simulations to match the observed data. The author was responsible for writing the paper as the first author.

Paper II: The author analysed the optical polarisation data observed with the Nordic Optical Telescope and participated in the discussion and writing of the paper.

Paper III: The author collected and analysed the VHE gamma-ray, optical, and radio data, and participated in performing the redshift estimation. The author participated in the coordination of the multi-wavelength observations and the polarisation modelling. The author was actively involved in the discussion and interpretation of the paper results as well as in writing the paper. The author was one of the corresponding authors and responsible for the publication coordination.

Paper IV: The author collected all the data, performed all the analyses, and was responsible for writing the paper as the first author.

Abbreviations

2D	Two-dimensional
ACZ	Acceleration and Collimation Zone
AGN	Active Galactic Nucleus
BL Lac	BL Lacertae object
BLR	Broad-Line Region
EC	External Compton
EHT	Event Horizon Telescope
FR I	Fanaroff-Riley type I galaxy
FR II	Fanaroff-Riley type II galaxy
FSRQ	Flat-Spectrum Radio Quasar
HE	High Energy
HSP	High Synchrotron Peaked blazar
IC	Inverse Compton
ISP	Intermediate Synchrotron Peaked blazar
IXPE	Imaging X-ray Polarimetry Explorer
LSP	Low Synchrotron Peaked blazar
MAGIC	Major Atmospheric Gamma Imaging Cherenkov
MHD	Magnetohydrodynamics
MWL	Multi-wavelength
NLR	Narrow-Line Region
PA	Polarisation Angle
PD	Polarisation Degree
PIC	Particle-in-cell
SED	Spectral Energy Distribution
SMBH	Supermassive Black Hole
SSA	Synchrotron Self-absorption
SSC	Synchrotron Self-Compton
VERITAS	Very Energetic Radiation Imaging Telescope Array System
VHE	Very High Energy
VLBI	Very Long Baseline Interferometry

Symbols

a	Black hole spin ($-1 \leq a \leq 1$)
c	Speed of light (2.997×10^{10} cm s^{-1})
B	Magnetic field strength (G)
B_{φ}	Toroidal magnetic field strength (G)
D	Diameter of the mirror or dish (m)
d_L	Luminosity distance (cm)
E	Energy (eV)
I	Intensity (Jy)
N	Number density of electrons (cm^{-3})
P	Probability ($0 \leq P \leq 1$)
P_{jet}	Jet power (erg s^{-1})
p	Momentum (g cm s^{-1})
p_x	Momentum along the x-axis (g cm s^{-1})
Q	Second Stokes parameter (Jy)
R	Emission region size (cm)
r_{H}	Event horizon radius (cm)
s	Spectral index of the electron distribution
S_{max}	Maximum flux density at certain frequency (Jy)
$T_{\mathrm{b,var}}$	Observed brightness temperature (K)
$T_{\mathrm{b,int}}$	Intrinsic brightness temperature (K)
t_{var}	Variability timescale (s)
U	Third Stokes parameter (Jy)
U_{B}	Magnetic energy density (erg cm^{-3})
U_{e}	Energy density of the electrons (erg cm^{-3})
u_1	Velocity of the shock plasma upstream (cm s^{-1})
u_2	Velocity of the shock plasma downstream (cm s^{-1})
u_{c}	Velocity of the magnetic mirror (cm s^{-1})
v	Velocity of the particle (cm s^{-1})
z	Redshift
z_{diss}	Dissipation distance (cm)

β	Velocity of a component in a jet

$\beta_{\rm app}$	Apparent transverse speed of a component in the jet
Γ	Bulk Lorentz factor
γ	Lorentz factor
$\gamma_{\rm b}$	Break electron Lorentz factor
$\gamma_{\rm max}$	Maximum electron Lorentz factor
$\gamma_{\rm min}$	Minimum electron Lorentz factor
δ	Doppler factor
$\delta_{\rm var}$	Variability Doppler factor
Θ	Angular resolution (rad)
θ'	Reconnection layer angle ($^\circ$)
$\theta_{\rm j}$	Jet opening angle ($^\circ$)
$\theta_{\rm obs}$	Viewing angle of the jet ($^\circ$)
λ	Wavelength (m)
ν	Frequency (Hz)
$\nu_{\rm peak}$	Synchrotron peak frequency (Hz)
ρ	Density (g cm^{-3})
ρ_m	Magnetic pressure (dyn cm^{-2})
σ	Magnetisation
τ	Optical depth
$\Phi_{\rm BH}$	Magnetic flux (G cm^2)

eV	Electron volt
Jy	Jansky ($10^{-26}\times$ W m^{-2} Hz^{-1})
mas	milliarcsecond
$M_\odot$	Solar mass (1.989×10^{33} g)
pc	Parsec (3.085×10^{18} cm)

1 Introduction

When gazing upon the night sky we see stars which, in a place dark enough, seem to form a pathway across the sky. With the help of a telescope, some of the objects that we thought as stars appear to be smudgy spots instead. That is because they are islands of stars, galaxies, and that pathway across the sky is a similar island, our own galaxy called the Milky Way. Galaxies consist of stars, gas, and dust, but today we know they also harbour something else in their hearts. In nearly all galaxies of the Universe, a black hole resides in their centre. Black holes are large concentrations of mass that have collapsed under their own gravity. Even light cannot escape from the gravitational attraction of these objects. In galaxy nuclei, the masses of black holes can be larger than $10^6 M_\odot$, and in such cases, they are called supermassive black holes (SMBHs). In the local Universe, the SMBHs are often dormant beasts that hide in the sea of stars. When peering deeper into space, to its more violent past, the SMBHs are actively accreting the surrounding matter around them into a disc. Such activity in the nucleus outshines the starlight of the galaxy itself. These objects are called active galactic nuclei (AGNs).

AGNs are among the most extreme phenomena in the Universe, seen even up to high redshifts. The tell-tale signatures that distinguish them from regular galaxies are a high luminosity across the entire electromagnetic spectrum and a contrasting small angular size (Salpeter 1964; Zeldovich & Novikov 1964; Lynden-Bell 1969). Their spectra often show luminous emission lines, and the observed emission is highly variable in all timescales from years to days, even down to minutes in rare cases. In a small fraction of AGNs, about 10 %, radio jets are seen extending far outside the host galaxy. Such signatures can only be caused by a tremendously massive and compact object such as an SMBH.

The activity within the nuclei of some galaxies is not the only evidence that we have of the existence of SMBHs. In nearby galaxies, it is possible to follow the proper motions of stars or megamasers in the nuclear regions. For example, in the case of the Milky Way, the stellar orbits around a central compact object have been traced and used to calculate its mass. In far-away AGNs, the short variability timescales of days or less are another way to discern that the emission must originate from a compact region although in the case of certain jetted sources such signatures complicate this conclusion. The emission lines observed from AGNs appear broadened, indicating high velocities of the gas clouds around the nucleus. The variations

of the broad emission lines, that is reverberation mapping, and for example, the width and the shape of Fe Kα line in the X-rays can be used to estimate the mass of the central object. These different estimation methods give the SMBHs in AGNs masses of 10^6–$10^9 M_\odot$ (e.g. Peterson 2014, for a review). Finally, the most direct evidence of a central SMBH comes from the observations of the Event Horizon Telescope (EHT) that has been able to image the 'shadows' of the black hole of the nearby radio galaxy M87 (Event Horizon Telescope Collaboration et al. 2019) and Sagittarius A* in the Milky Way (Event Horizon Telescope Collaboration et al. 2022).

The emission signatures that are observable from AGNs reveal the structure of the nuclear regions. The left side of Fig. 1 shows the typical anatomy of a jetted AGN. The central SMBH is surrounded by an accretion disc, which is seen as a thermal blackbody component ('big blue bump') in the optical and ultraviolet wavelengths (blue curve in Fig. 2). An observed hard X-ray continuum from some AGNs hints at the existence of a hot corona located near the accretion disc. Further out from the accretion disc is the broad-line region (BLR) that produces the luminous broad emission lines observed in some AGNs. The typical lines (e.g. Lyα, CIV, CIII, MgII) observed from these clouds closest to the SMBH have line widths corresponding to speeds of 1000–25000 km/s. Beyond the BLR are the clouds of the narrow-line region (NLR; e.g. OIII, OII, OI, and Hβ) with widths corresponding to speeds of 200–900 km/s. Both the BLR and NLR lines are a result of reprocessed thermal emission from the AGN. Surrounding the nucleus and the BLR, there is thought to exist a dusty torus that appears as a thermal component due to the reradiated emission of the accretion disc (see orange curve in Fig. 2). The exact structure of the torus is not known but because some edge-on AGNs, in which the torus essentially should obscure the nucleus, sometimes show broad emission lines, it is thought to be clumpy and irregular (Netzer 2015). In a small fraction of AGNs, relativistic jets can be seen extending from the poles of the SMBH. The radiation from jets in parsec (pc) scales is seen as synchrotron emission in the radio-to-X-ray wavelengths (red curve in Fig. 2), and in the higher energies, from X-rays to very high-energy (VHE, $E > 100$ GeV) gamma rays, their emission is thought to be produced by the inverse Compton (IC) mechanism, in which low-energy photons gain energy from relativistic electrons (purple curve in Fig. 2). The exact mechanism of the higher energy emission is, however, still under debate, and will be further discussed in Chapter 4.2.1.

Zooming further out from the nucleus, as seen on the right in Fig. 1, the host galaxy encloses the active nucleus. The starlight from the host emits a thermal component (green curve in Fig. 2). The large-scale jets in AGNs can extend far outside the host galaxy and often reach kiloparsec (kpc), sometimes megaparsec scales (Mpc, Hardcastle & Croston 2020). In this range, the emission from the jet in the lower energies is again caused by synchrotron radiation. The higher energy emission (X-rays and beyond) is likely caused either by synchrotron or IC off of cosmic

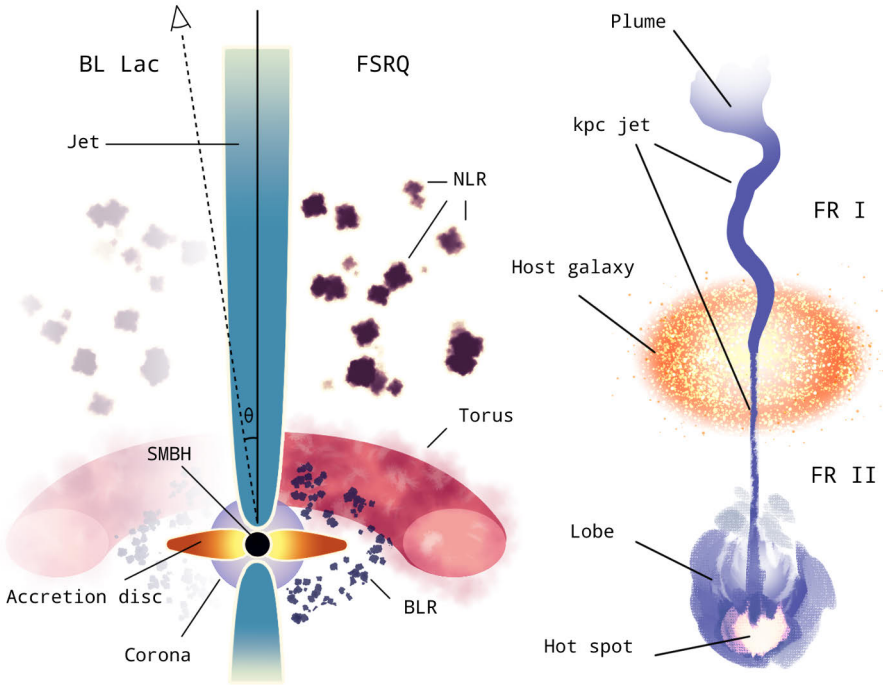

Figure 1. Structure of a jetted AGN on the left. When the jet is viewed at a small angle ($<10°$), the source is called a blazar. In BL Lacs, the torus, BLR, and NLR are weak or absent, whereas in FSRQs these components are expected to exist and broad emission lines are observed. On the right, the two large-scale jet morphologies are depicted. Blazars reside in massive elliptical galaxies, and the jets in FR I galaxies are a result of weak jet power, whereas the FR II galaxies represent the higher jet power type. Figure by Jenni Jormanainen.

microwave background photons although the latter might not be relevant for many sources (Meyer & Georganopoulos 2014). Based on the jet power and the large-scale jet morphology, jetted AGNs are divided into Fanaroff-Riley I (FRI) and Fanaroff-Riley II (FR II) types, the former representing the lower and the latter the higher power objects (Fanaroff & Riley 1974). The right side of Fig. 1 shows the two kinds of morphologies seen from these AGNs. The jets in FR I sources are more prominent, but they are often seen stalling within the interstellar medium of the host galaxy, thus becoming asymmetric and ending in hazy plumes. In FR II sources, the jets are thin and neatly collimated, often appearing to be one-sided due to relativistic effects, and show bright hotspots and radio lobes at the end of usually both jets. In the current models where the jets are magnetically launched, the radial magnetic flux and the black hole spin are thought to determine the power of the jet, directly affecting the appearance of the resulting jet. Because the jet power is seen changing

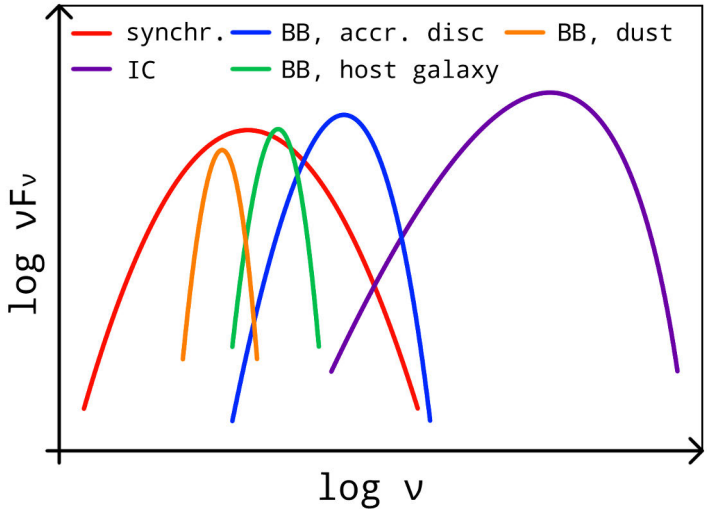

Figure 2. The emission components typically present in the spectral energy distributions of AGNs. In blazars, the broadband spectrum is mostly dominated by the synchrotron and IC emission from the jet. Figure by Jenni Jormanainen.

in some AGNs, but the spin of the black hole is not expected to change within our lifetime, the magnetic flux must change and therefore the accretion process as well. Magnetohydrodynamics (MHD) simulations with radiative transfer have been able to shed some light on this disc-jet connection and the differences between the two jet types (see Davis & Tchekhovskoy 2020, for a review). There are also observations supporting the intrinsic differences (Laing et al. 1994) although it is also debated that the differences may be external and relate to the host galaxy properties (De Young 1993; Owen & Ledlow 1994) or be an effect of both (Tchekhovskoy & Bromberg 2016).

Based on the emission features that we observe, AGNs are divided into a vast and growing collection of classes. One method is based on their radio loudness. Radio loudness can be assessed based on a limit on the flux density of the radio flux, the ratio of the radio-to-optical flux, or the spectral luminosity of the radio emission (Kellermann et al. 2016). Radio-loud sources always have powerful radio jets while radio-quiet sources were originally thought to be unable to launch jets. Radio-loud AGNs are generally known to reside in massive elliptical galaxies (Kotilainen et al. 1998; Nilsson et al. 2003), but in recent years, jets have also been observed in some Seyfert galaxies, specifically in NLS1 types (e.g. Lähteenmäki et al. 2017; Järvelä et al. 2018; Varglund et al. 2022), challenging the current view of the host galaxy properties of jetted AGNs. The division into quasars (quasi-stellar radio-source) or QSOs (quasi-stellar object) and Seyfert galaxies has been made in the past based on their bolometric luminosities with quasars having higher luminosities

than Seyfert galaxies. An even lower state of activity can be recognised in nearby galaxies, typically called LINERs (Low-Ionisation Narrow-Line Region galaxies), that represent the borderline case between normal and active galaxies (Jogee 2006). A division based on emission lines can also be made; type 1 AGNs show both broad and narrow emission lines whereas type 2 AGNs present only narrow emission lines. Essentially, this is thought to be an effect of the angle at which the galaxy is seen; the BLR can be hidden by the torus in those galaxies viewed edge-on.

The various classification methods are useful in identifying AGNs, and broad strokes can be drawn to unify the various subtypes with the dichotomy to radio-loud and radio-quiet sources or with varying source inclinations (Urry & Padovani 1995), but the real picture is more complex and requires an understanding of the evolutionary history of galaxies and AGNs together. This is demonstrated by, for example, the existence of the LINERs, the lowest state of AGN activity; Narrow Line Seyfert 1 galaxies that can possess a low power jet against the expectations based on the typical properties of Seyfert galaxies; and changing-look AGNs, in which the nucleus can sometimes be obscured or the emission properties can completely disappear and appear again. The true unification of AGNs therefore needs to account for the intrinsic differences as well as those caused by the orientation.

1.1 Blazars

When one of the jets of a radio-loud AGN is viewed closely aligned with our line of sight ($<10^{\circ}$, Lähteenmäki & Valtaoja 1999), these objects are called blazars (Blandford & Rees 1978; Urry & Padovani 1995). This special inclination makes the jet appear much brighter, Doppler boosted, compared to their misaligned counterparts. Based on whether broad emission lines are seen in their spectrum, blazars can be divided into BL Lacertae objects (BL Lacs) whose lines are weak or absent and flat-spectrum radio quasars (FSRQs) with luminous broad lines (with rest-frame equivalent widths >5 Å, e.g. Scarpa & Falomo 1997; Ghisellini et al. 2011). BL Lacs are thought to correspond to the FR I galaxies and FSRQs to the FR II galaxies (Ghisellini et al. 2009a), and it is thought that BL Lacs and FSRQs differ in their accretion processes (e.g. Baum et al. 1995; Landt & Bignall 2008; Ghisellini et al. 2009b; Kharb et al. 2010). Because the jets in BL Lacs represent the lower power kind, the weak or absent emission lines even during low activity states in some sources have been interpreted as near absence of structures such as a torus or a BLR (Chiaberge et al. 1999). Some complication to the blazar classification is introduced through 'masquerading' BL Lacs, such as the prototype itself, that show no broad emission lines during high activity periods but reveal them when the non-thermal jet emission is more quiescent (e.g. Vermeulen et al. 1995; Giommi et al. 2013).

Blazars can be further divided based on the peak frequency of the synchrotron emission bump in their spectral energy distribution (SED). This gives rise to the cat-

egories of high (HSP, $\nu_{\rm peak} \gtrsim 10^{15}$ Hz), intermediate (ISP, 10^{14} Hz $\lesssim \nu_{\rm peak} \lesssim 10^{15}$ Hz), and low synchrotron peaked blazars (LSP, $\nu_{\rm peak} \lesssim 10^{14}$ Hz). In this categorisation, HSPs and ISPs are always BL Lacs and LSPs are BL Lacs and FSRQs (Abdo et al. 2010a). These categories are often described together as the debated blazar sequence where the more luminous sources have lower synchrotron peak frequencies and higher Compton dominance of the high energy component (Fossati et al. 1998). The simple sequence has since been challenged, and it appears more likely that the spectral type does not only depend on the source jet power. Instead, the sources seem to be divided into low and high jet power sources where the lower power sources can either present strong or weak jets based on their accretion rates (Meyer et al. 2011). Some BL Lacs have also been seen extending their synchrotron peak to MeV energies, and some authors have suggested a category above the HSPs for such sources (Ghisellini 1999; Giommi et al. 2001; Bonnoli et al. 2015).

This thesis focusses on investigating the properties of relativistic jets using various methods. The jets can best be studied in blazars where the jet is seen pointing almost directly towards us, making the emission Doppler boosted, overpowering the other emission components of a typical AGN. In Papers I and II of this thesis, the archetypical HSP BL Lacs Markarian 421 (Mrk 421) and Markarian 501 (Mrk 501) were studied, whereas VER J0521+211 in the focus of Paper III has typically been classified as either an ISP or an HSP. The blazar OJ 287 studied in Paper IV typically has its synchrotron peak within the range of LSPs, and its observed emission lines are weak. Both Mrk 421 and Mrk 501 are bright and nearby blazars that are regularly observed via numerous monitoring programmes from radio to VHE gamma rays. In the papers of this thesis, they were used to study the acceleration mechanisms of the jet, the aforementioned attributes making them ideal objects for this. VER J0521+211 was observed flaring in the VHE gamma rays in spring 2020, and its broad-band spectrum was studied during this time. OJ 287 is the likeliest candidate to host an SMBH binary to date, and the several events observed in its jet between 2015 and 2017 were recontextualised using MWL polarisation observations.

The structure of this thesis is following. In Chapter 2 relativistic jets, their launching, and structure are described in more detail. In Chapter 3 some of the relevant acceleration mechanisms are introduced. In Chapter 4 central methods to constrain jet parameters are presented. Chapter 5 focusses on the methods to simulate fast variability in blazar jets. In Chapter 6 the results of each paper are summarised.

2 Relativistic jets

The matter that is accreted by the SMBH in the nuclei of active galaxies does not only end up feeding the central engine but can sometimes be pushed outwards in the form of powerful collimated outflows called jets. The large-scale jets extending far outside the host galaxy were described in the previous chapter. This chapter focusses on the pc-scale distances from the SMBH where the relativistic part of the jet is seen.

Whereas the kpc-scale jets (subfigure *a* in Fig. 3 in the case of M87) can be imaged with radio, optical, and X-ray instruments (e.g. in M87: Curtis 1918; Biretta et al. 1999; Wilson & Yang 2002; Meyer et al. 2013, in 3C 273: Rees 1966; Meyer et al. 2016), observing the jet within pc-scale distances from the SMBH (that is inside the host galaxy) is possible only in radio frequencies using very long baseline interferometry (VLBI). In VLBI, several antennae separated by large distances emulate a single telescope, reaching sub-milliarcsecond resolutions. In the pc scales, usually, only one of the jets is seen (subfigures *b–e* in Fig. 3). Because the jet plasma is moving near the speed of light, the emission from the jet is relativistically beamed, Doppler boosted, and appears brighter on the side more inclined towards the observer. The other jet directed away from the observer then becomes de-boosted and often cannot be seen at all. The Doppler boosting factor, δ, of an emission region within the pc-scale jet depends on the bulk Lorentz factor, $\Gamma = (1 - \beta^2)^{-1/2}$, the speed, $\beta = v/c$, and the viewing angle, $\theta_{\rm obs}$, of the jet and is given by (e.g. Böttcher et al. 2012a)

$$\delta = \frac{1}{\Gamma(1 - \beta \cos \theta_{\rm obs})}. \tag{1}$$

In blazars, the jet emission is strongly Doppler boosted due to the small viewing angle, and the observed emission is thus dominated by that of the jet, often overpowering the rest of the nucleus and the host galaxy.

Zooming in towards the SMBH, within some tens of parsecs from the central engine (see also subfigures *d–e* in Fig. 3), the jet starts to show substructures. A simplified schematic of the pc-scale jet is shown in Fig. 4. Limb-brightened morphologies have been observed in VLBI observations (e.g. Giroletti et al. 2004; Piner et al. 2009; Nagai et al. 2014; Giovannini et al. 2018). This is typically thought to be a slower moving sheath surrounding the thin, faster-moving spine of the jet (Ghisellini et al. 2005). This spine-sheath structure has also been suggested to explain the

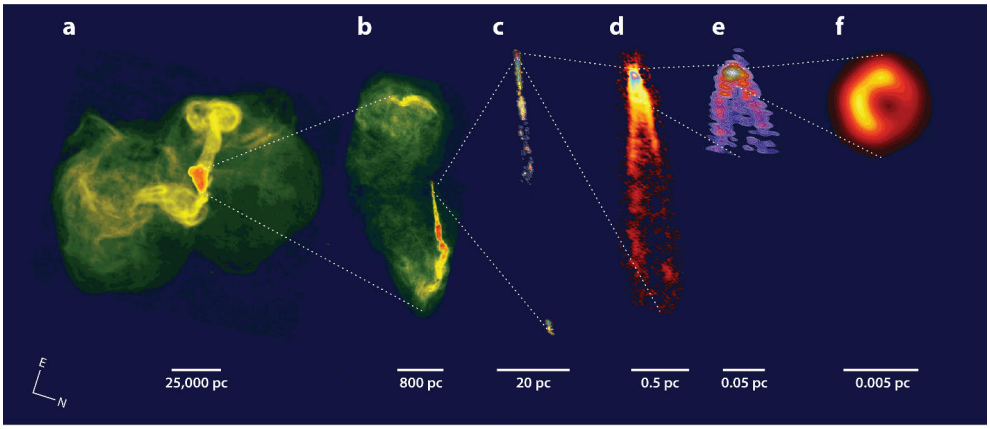

Figure 3. The jet of the FR I radio galaxy M87 on different scales from kpc to sub-pc scales. *a*) kpc jets showing the outer lobes and remnant lobes of past jet activity *b*) jet within the galaxy showing also the inner lobes; *c*) pc-scale jet and a bright optical feature; *d*) innermost jet in the sub-pc scales; *e*) jet launching region; and *f*) black hole and the accretion disc. Image from Blandford et al. (2019) with permissions from (*a–b*) NRAO, (*c*) Cheung et al. (2007), (*d*) Walker et al. (2018), (*e*) Kim et al. (2018), and (*f*) Event Horizon Telescope Collaboration et al. (2019).

so-called 'Doppler crisis'. For some HSP blazars, the jet speeds obtained through VLBI observations appear very slow, but these sources can produce fast variability in the higher energies (optical to VHE gamma-rays). In these cases, the Doppler factor derived from the slow jet speed is in conflict with the high Doppler factors that are required by such fast variations (see also Chapters 4.2.1 and 4.2.2). This dilemma has spawned other suggestions for substructures within the jet where the jet flow could be faster, such as jet-in-jet models (Giannios et al. 2009), or magnetic reconnection layers aligned in a way that offers further boosting to the observed emission (Christie et al. 2019, see also Paper I).

In some jetted AGNs, plasma 'blobs' or 'knots' moving down the jet appear to surpass the speed of light, reaching even up to $50c$ in some sources (Lister et al. 2016). This phenomenon known as superluminal motion is a combined effect of the geometry (the jet is viewed from a small angle with regards to the observer) and the relativistic jet speeds (of the order $0.98c$). This is typically observed in the pc-scale jets where the jet speeds are still relativistic, but superluminal motion has also been observed in kpc scales (within 2 kpc) for example in M87 (Biretta et al. 1999; Meyer et al. 2013).

Moving further inside, within some parsecs from the SMBH, VLBI observations show a bright, stationary region typically known as the 'core'. The location of this core depends on the observed wavelength as the lower radio frequencies become optically thin further down the jet compared to higher frequencies. At 43 GHz, this

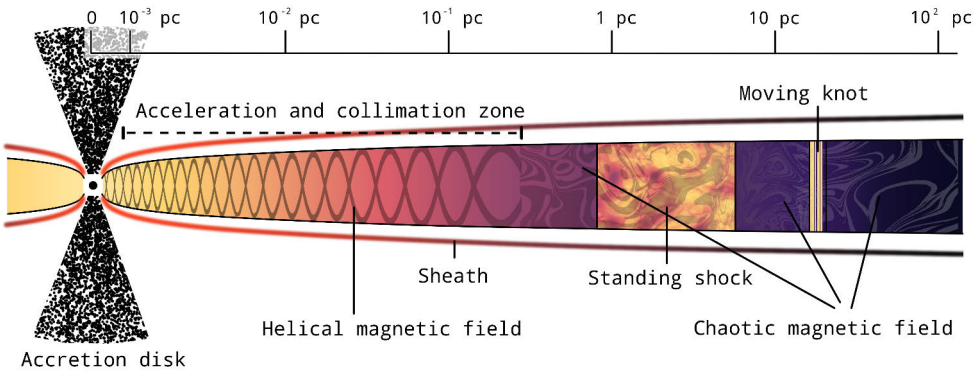

Figure 4. Schematic showing the substructures of a pc-scale jet. Figure by Jenni Jormanainen, adapted from Marscher (2005).

observed radio core is often thought to be a standing shock (Daly & Marscher 1988) that forms when the jet reaches its terminal velocity and the speed of the bulk flow changes (see Fig. 4).

The last sub-parsec before the SMBH is only seen for a small number of nearby sources due to the required high spatial resolutions (e.g. in NGC 1275: Savolainen et al. 2023). In these regions, the jet is thought to accelerate through the conversion of the magnetic and thermal energy into the bulk motion of plasma (Li et al. 1992; Beskin & Nokhrina 2006) and collimate with the help of an external pressure (Komissarov et al. 2007; Lyubarsky 2009; Nakamura et al. 2018). This region of the jet known as the acceleration and the collimation zone (ACZ, see Fig. 4) has been observed for some AGNs (Junor et al. 1999; Kovalev et al. 2007; Boccardi et al. 2019) and has been thought to extend to distances $\lesssim 10^5$ gravitational radii from the SMBH (Junor et al. 1999; Biretta et al. 2002; Marscher et al. 2008; Asada & Nakamura 2012). It is also thought that the jet flow transforms from a magnetically dominated parabolic jet to a particle-dominated conical one within the ACZ. The transition of the jet shape is expected to happen when the bulk kinetic energy of the jet plasma becomes equal to its Poynting flux (Komissarov et al. 2009; Lyubarsky 2009), and such shape transitions have been observed for some sources (e.g. Kadler et al. 2004; Böttcher et al. 2005; Pushkarev et al. 2017; Kovalev et al. 2020). It is also possible that a change in the external pressure affects this change in the jet shape (Vlahakis 2015; Komissarov et al. 2007, 2009; Lyubarsky 2009, 2010).

The jets are thought to be launched from the vicinity of the SMBH powered by the accretion of matter. The exact mechanism of jet launching is not known, and it is difficult to study because of the extremely small scales. In fact, the SMBH in the centre of the host galaxy has so far been imaged only in M87 (see subfigure *f* in Fig. 3, Event Horizon Telescope Collaboration et al. 2019) and Milky Way (Event Horizon Telescope Collaboration et al. 2022). However, the jet launching is thought

to act through the transformation of the rotational energy of a spinning (Kerr) black hole (Blandford & Znajek 1977) or an accretion disc (Blandford & Payne 1982). These mechanisms both work in a similar manner by electromagnetically extracting the angular momentum of the black hole or the accretion disc. This scenario can be analogously described by a perfectly conducting sphere that is connected to the ambient medium, perfectly conducting 'ceiling', by a magnetic field line. The initially poloidal magnetic field lines are twisted into a helical morphology as the sphere rotates, creating a magnetic spring that pushes against the ceiling with an effective pressure $\rho_{\rm m} = B_{\varphi}^2/8\pi$, where B_{φ} is the strength of the toroidal magnetic field. Once the strength of the toroidal magnetic field greatly surpasses that of the poloidal field, the conducting ceiling and the plasma attached to it are pushed away and accelerated, forming a jet along the rotational axis of the sphere (Davis & Tchekhovskoy 2020). First derived by Blandford & Znajek (1977), the jet power of a slowly spinning black hole is connected to its spin and the magnetic flux. Later, numerical simulations were used to more accurately apply this also to rapidly spinning black holes (Komissarov 2001)

$$P_{\rm jet} = k(a/r_{\rm H})^2 \Phi_{\rm BH}^2 c \times f(a), \tag{2}$$

where k is a dimensionless proportionality factor, $-1 \leq a \leq 1$ is the black hole spin, $r_{\rm H}$ is the event horizon radius, $\Phi_{\rm BH}$ is the magnetic flux of the black hole, and $f(a)$ is a higher-order correction function for spin values up to $a = 1$. With the latest advancements in the field (such as the EHT), the regions closest to the SMBH have become more accessible for studying jet launching. The helical magnetic field of the jet launching region is thought to persist in the jet within sub-pc distances (see subfigure *d* in Fig. 3 and also Fig. 4). Because the non-thermal synchrotron emission is intrinsically polarised, polarisation observations can be used to study the morphology of the magnetic field and the jet launching. Polarisation observations were used in three papers of this thesis; II, III, and IV, and will be further discussed in Chapter 4.3.

While our understanding of the jet structure has leapt forward with the more and more detailed observations offered by the VLBI method, there are still questions left unanswered. The ACZ has been observed for some sources, and it could be expected that after this region the plasma begins to cool down and emit only in the lower wavelengths as the jet decelerates. However, some jets have been seen accelerating even beyond 100 pc (Homan et al. 2015). Quasi-stationary features have been observed beyond the radio core in the pc-scale jets through VLBI (Jorstad et al. 2005; Marscher et al. 2008; Lister et al. 2013; Cohen et al. 2014; Gómez et al. 2016), and it is possible that these shocks appear if the jet continues to accelerate beyond the initial ACZ via for example a striped jet model (Giannios & Uzdensky 2019) and are thus recollimation shocks (Gómez et al. 1995; Mizuno et al. 2015). Such recolli-

mation shocks could be ideal sites to accelerate particles to the highest energies (up to TeV energies in gamma rays), and it has been suggested that a passage of a blob through a recollimation shock could provide the needed turbulence for this (MAGIC Collaboration et al. 2018; Lico et al. 2022). This kind of scenario was suggested in Paper IV. However, it is not certain whether, for example, magnetic reconnection could take place in a shocked, particle-dominated region (see discussion in Chapter 5 and references therein).

The exact particle composition of the jet is not known, but generally, it is assumed to consist of leptons. If relativistic hadrons are present within the jet, it is possible that the higher energy emission is a result of, for example, proton-photon interaction. Observations of high-energy neutrinos have been made possible with the IceCube neutrino observatory. The origin of the astrophysical neutrinos has been studied in more detail in recent years, and blazars with their great potential to accelerate particles are one of the most promising candidates. The first evidence of this possible connection came with the coincident neutrino observation with the blazar TXS 0506+056 (detection at a 3.5σ significance level: IceCube Collaboration et al. 2018; Ansoldi et al. 2018). While promising, further population studies (e.g. Plavin et al. 2020; Giommi et al. 2020; Hovatta et al. 2021; Suray & Troitsky 2024; Kouch et al. 2024, and references therein) have shown only a weak connection between blazars and neutrinos. Additionally, theoretical estimations of the neutrino flux from BL Lacs expect modest rates even from the most powerful sources (Oikonomou et al. 2019). Another likely candidate could be Seyfert galaxies (NGC 1068: IceCube Collaboration et al. 2022). The existence of relativistic hadrons within the blazar jets would also render them as candidate emitters of ultra high-energy cosmic rays (Hillas 1984; Norman et al. 1995; Fang & Murase 2018; Rodrigues et al. 2018). Solving questions about the particle composition of the jet and the jet magnetic field and structure via different methods are central to answer which particle acceleration mechanisms are present in the jet and where they act. The jet composition and emission components are further discussed in Chapter 4.2.1, and were also studied in Paper III in the context of SED modelling.

3 Acceleration mechanisms

Charged particles can be accelerated in electromagnetic fields where the Lorentz force transforms the energy of the electromagnetic field into the energy of the particle. Relativistic jets in AGNs are the grandest particle accelerators occurring in nature. Blazars, in which the jet is pointing closely along our line of sight, are especially interesting because the broadband emission that we observe from them is largely dominated by the jet. Their emission appears variable in all timescales and wavelengths. These variations are often called flares. Typically, the variability of the emission observed from blazars (discussed in more detail in Chapter 4.2.2) is slow (variations within years to months) in the radio and optical bands with optical presenting also fast variability (days and shorter) on top of the slower trends. Flares in the lower energies are thought to result from shocks propagating in the jet and such models are able to explain these signatures well (e.g. Marscher & Gear 1985; Hughes et al. 1985; Spada et al. 2001; Lindfors et al. 2006; Joshi & Böttcher 2007; Graff et al. 2008; Di Gesu et al. 2022, see also Paper II). The faster variability (in intra-night timescales) present from optical (e.g. Raiteri et al. 2023; Tripathi et al. 2024) to VHE gamma-ray bands (e.g. Aharonian et al. 2007; Albert et al. 2007; Aleksić et al. 2011, 2014c; Abeysekara et al. 2018; Acciari et al. 2020) is more tricky to explain. The observed variations are expected to reflect the size of the emitting regions (see Chapter 4.2.2). Observing minute-scale variability means that the observed emission comes from a region whose size is smaller than the event horizon of a typical SMBH with a mass of $10^9 M_\odot$. In addition, the opening angles of the jets have been estimated to be 0.1–9.4° (with a median of 1.3°, Pushkarev et al. 2017), meaning that fast flares must originate from a region that is smaller than the jet cross-section (see Chapter 4.2.2). In the case of fast variability, models such as magnetic reconnection (Giannios et al. 2009; Giannios 2013) could produce acceleration within a small region.

Because the observed multi-wavelength (MWL) emission from blazar jets varies across all timescales, it can be expected that the origins of these emissions are not entirely co-located (see Chapter 2). It appears likely that there must be several mechanisms that accelerate particles in the jet. In addition, these acceleration mechanisms must be able to account for the observed variable and strong MWL polarisation signatures as well as the power-law non-thermal particle spectrum. For observed synchrotron spectra, the electrons are expected to have a power-law distribution of the

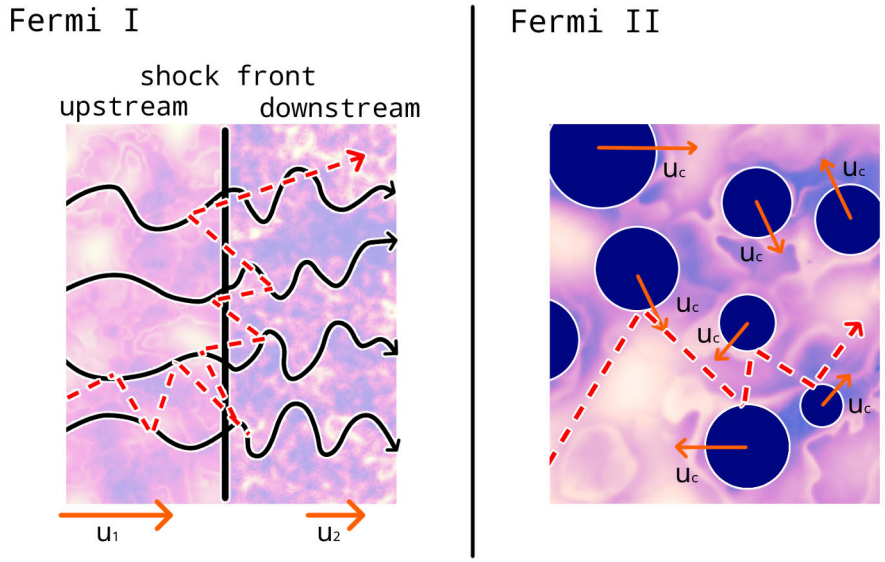

Figure 5. Schematic of the first-order Fermi acceleration (diffusive shock acceleration) on the left. Plasma turbulence is depicted in black arrows. In both panels, bulk speeds are depicted with orange arrows and the particle paths in dashed red arrows. The particle will first diffuse in the upstream before crossing the shock front. The particle will experience several shock-crossings, gaining energy in the process, before exiting the shocked region. On the right, schematic of the second-order Fermi (stochastic) acceleration. The particle collides with magnetised mirrors with random velocities, gaining energy in the multiple head-on collisions. Figure by Jenni Jormanainen, adapted from Matthews et al. (2020).

form

$$N(E)dE \propto E^{-s}, \tag{3}$$

where $N(E)$ is the number density of electrons at a certain energy, E is the energy of the particles, and s is the spectral index (Matthews et al. 2020).

In Paper I the observed variability signatures of blazars are analysed in the context of magnetic reconnection, and in Paper II different acceleration mechanisms are compared with MWL polarisation signatures. In this Chapter, the most typical acceleration mechanisms are described, and some of the relevant models that utilise these mechanisms are introduced.

3.1 Shock acceleration

Shock acceleration, or the first-order Fermi acceleration, is thought to be one of the main acceleration mechanisms for particles in relativistic jets. A shock front forms

when the flow velocity exceeds the sonic velocity of the medium, meaning a region where the speed of the jet flow changes from supersonic in the upstream to subsonic in the downstream. The quasi-stationary features observed in pc-scale jets through VLBI are thought to be recollimation shocks born when the jet flow decelerates and accelerates again. The moving jet components can also act as a source of disturbance in the jet flow, creating shock waves (Marscher & Gear 1985). The dominating mechanism of shock acceleration in relativistic jets is likely diffusive shock acceleration (Axford et al. 1977; Krymskii 1977; Bell 1978; Blandford & Ostriker 1978). In this mechanism, the relativistic particles of the upstream diffuse via collisions with the irregularities of the turbulent, magnetised plasma. As the particles cross the shock front, the slower downstream plasma turbulence appears to be approaching in the rest frame of the upstream plasma. This means that the particle crossing the shock front upstream or downstream experiences a head-on collision with the plasma moving at velocity $v = u_1 - u_2$ (see panel on the left in Fig. 5). The energy of the particle upstream can be expressed in the downstream frame as (see, e.g. Longair 1994)

$$E' = \gamma(E + p\cos\theta\, v), \tag{4}$$

where E and p are the energy and the momentum of the particle upstream, θ is the angle between the shock normal and the crossing path, and γ is the Lorentz factor which for a non-relativistic shock is 1. If the particle is relativistic $E = pc$. Then the energy of the particle becomes

$$E' = E + \frac{E}{c} v\cos\theta. \tag{5}$$

The energy gain per half-cycle can now be expressed as

$$\frac{\Delta E}{E} = \frac{v}{c}\cos\theta. \tag{6}$$

Because the particles will be isotropised by the plasma irregularities in this process, they have the probability to cross the shock front

$$P(\theta) = 2\sin\theta\cos\theta\, d\theta. \tag{7}$$

The average energy gain per half-cycle is obtained by averaging over the probability distribution

$$\left\langle \frac{\Delta E}{E} \right\rangle = 2\frac{v}{c}\int_0^{\frac{\pi}{2}} d\theta\cos^2\theta\sin\theta = \frac{2}{3}\Big(\frac{v}{c}\Big). \tag{8}$$

Because it is more probable that the particles will cross the shock back upstream instead of escaping the acceleration region, the energy gain of the full cycle is twice the energy gain of the half cycle.

$$\left\langle \frac{\Delta E}{E} \right\rangle = \frac{4}{3}\left(\frac{v}{c}\right). \tag{9}$$

Typically, the particles experience several shock-crossings before escaping the shocked region, leading to a significant increase in the particle energies (up to TeV energies).

Many models utilising shock acceleration are generally able to reproduce the slower variability in the radio and optical bands. They are also able to account for the non-thermal power-law particle spectra with indices $s \sim 2$ typically seen for blazar jets (Achterberg et al. 2001; Spitkovsky 2008; Summerlin & Baring 2012) although the hard spectral shape during flaring in some sources poses challenges to shock models (Zhang et al. 2017). Shocks are expected to compress and order the turbulent magnetic field and, thus, manage to explain the high polarisation degrees seen in many blazars (Hughes et al. 1985). In Paper II, the higher X-ray polarisation degree compared to that seen in the optical and radio bands was taken as evidence of shock acceleration because the X-rays originate closer to the acceleration site where the magnetic field is more ordered. However, it is not clear if shocks can account for the $>180^\circ$ polarisation angle (PA) swings (Zhang et al. 2018). It is also possible that the efficiency of shock acceleration is reduced in strongly magnetised flows (Kennel & Coroniti 1984; Sironi et al. 2015), but turbulent shock upstreams could offer a solution to this problem (Bresci et al. 2023; Demidem et al. 2023).

3.2 Stochastic acceleration

The other mechanism thought to be acting in the relativistic jets is similarly related to plasma turbulence. Instead of gaining energy through shock crossings, the particles receive energy by interacting with moving magnetised clouds. In relativistic jets, these clouds can also be the plasma turbulence with random velocities. This is known as stochastic acceleration or the second-order Fermi acceleration. As demonstrated on the right in Fig. 5, the particle collides with random velocities considered as 'magnetic mirrors'. Assuming that the magnetic mirror is massive, its velocity u_c remains unchanged in the collision. Then the energy of the particle in the magnetic mirror's frame is (see, e.g. Longair 1994)

$$E' = \gamma\Big(E + u_\mathrm{c} p\cos\theta\Big), \tag{10}$$

where θ is the angle between the mirror normal and the direction of the particle. The momentum of the particle along the x-axis in the mirror frame is

$$p'_x = p'\cos\theta' = \gamma\left(p\cos\theta + E\frac{u_c}{c^2}\right). \tag{11}$$

Because the particle's energy is conserved in the collision, its direction of momentum is simply reversed. After the collision, the energy of the particle expressed in the observer's frame is

$$E'' = \gamma\left(E' + u_c p'_x\right) = \gamma^2 E\left(1 + 2\frac{pu_c\cos\theta}{E} + \frac{u_c^2}{c^2}\right). \tag{12}$$

The particle's momentum can be expressed as $p = Ev/c^2$. This gives then

$$E'' = \gamma^2 E\left(1 + 2\frac{vu_c\cos\theta}{c^2} + \frac{u_c^2}{c^2}\right). \tag{13}$$

The change in energy is then the difference between the energy before and after the collision

$$\Delta E = E'' - E = \gamma^2 E\left(1 + 2\frac{vu_c\cos\theta}{c^2} + \frac{u_c^2}{c^2} - \frac{1}{\gamma^2}\right). \tag{14}$$

Inserting $1/\gamma^2 = 1 - u_c^2/c^2$ this becomes

$$\Delta E = \gamma^2 E\left(1 + 2\frac{vu_c\cos\theta}{c^2} + \frac{u_c^2}{c^2} - 1 + \frac{u_c^2}{c^2}\right). \tag{15}$$

Assuming that the mirror is non-relativistic so that $\gamma \approx 1$, this simplifies to

$$\Delta E = 2E\frac{u_c}{c}\left(\frac{v\cos\theta}{c} + \frac{u_c}{c}\right). \tag{16}$$

The probability that the scattering occurs head-on for a relativistic particle is given by

$$P(\theta) = \left(1 + \frac{u_c}{c}\cos\theta\right). \tag{17}$$

When the particle is relativistic $v \approx c$. Averaging over all angles between 0 and π and substituting $x = \cos\theta$ and $\beta = u_c/c$ gives

$$\left\langle \frac{\Delta E}{E} \right\rangle = \frac{\int P(\theta) \frac{\Delta E}{E} \sin\theta \, d\theta}{\int P(\theta) \sin\theta \, d\theta} = 2 \frac{u_c}{c} \frac{\int_{-1}^{1} (x + \beta + \beta x^2 + \beta x^2) dx}{\int_{-1}^{1} (1 + \beta x) dx}. \quad (18)$$

Integrating the above we finally get

$$\left\langle \frac{\Delta E}{E} \right\rangle = \frac{8}{3} \left(\frac{u_c}{c} \right)^2, \quad (19)$$

hence the name 'second-order'. This makes stochastic acceleration rather slow, requiring a much longer time for the particle to remain confined within the acceleration region in order to gain high energies (Matthews et al. 2020).

In special conditions, stochastic acceleration is also able to account for the non-thermal power-law spectra of blazars, although typically the obtained spectral indices are <2 (Virtanen & Vainio 2005). In addition, while turbulent random walk may account for some PA rotations, it is unlikely to cause the long and smooth PA swings often seen in blazars and, for example, those rotations which are associated with gamma-ray flares (Blinov et al. 2015). It is possible that stochastic acceleration still takes place in the wake of shocks where it could act as a complementing mechanism, creating spectra of various shapes (Virtanen & Vainio 2005) and lowering the polarisation degree that in shock models can often exceed 40% which is possible but rarely seen in blazars (Scarpa & Falomo 1997; Morozova et al. 2014; Angelakis et al. 2016; Smith 2017).

3.3 Magnetic reconnection

In the relativistic magnetised plasmas such as in blazar jets, magnetic reconnection can take place when tearing instabilities (e.g. Loureiro et al. 2007; Bhattacharjee et al. 2009; Uzdensky et al. 2010; Huang & Bhattacharjee 2012; Loureiro et al. 2012; Ni et al. 2015) or plasma turbulence (e.g. Zhdankin et al. 2017; Comisso & Sironi 2018, 2019; Nättilä & Beloborodov 2021) twist the ordered magnetic field. As illustrated in Fig. 6, field lines of opposite directions are pushed together. The field lines become tearing unstable and break the initial line, reconnecting with the line of opposing direction. In this event, magnetic energy is released in an explosive manner into heat and bulk kinetic motion of plasma. The reconnection event can then lead to first-order Fermi acceleration of the particles in the reconnection region if they cross the convergent flow between the two regions of opposite magnetic polarity, acting similar to a shock front (Matthews et al. 2020).

Magnetic reconnection models have been shown to recreate the non-thermal power-law shapes with spectral indices ~ 2 (e.g. Zhang et al. 2021, 2023; Werner

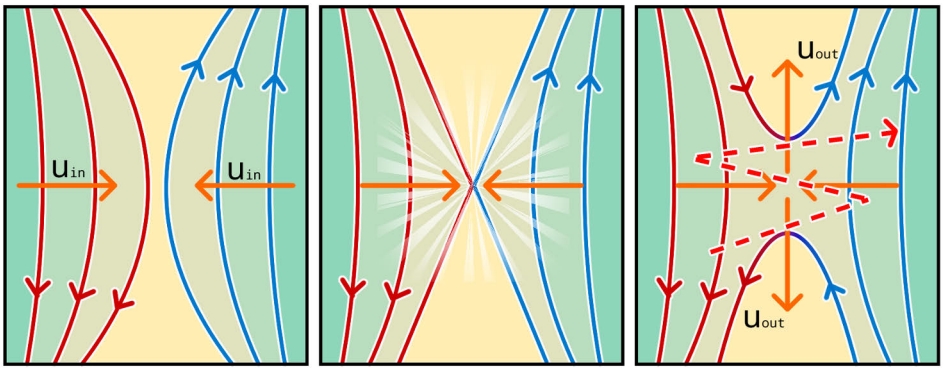

Figure 6. Schematic of magnetic reconnection from left to right; magnetic field lines of opposite directions are pushed closer to each other causing an influx of plasma towards the converging field lines. Magnetic energy is released as the field lines break (X-point) and reconnect with the opposing side. The inflowing plasma is directed out as magnetised islands. Particle acceleration occurs similarly to Fermi I as repeated crossings through the convergent plasma flow. Bulk velocities of the plasma are shown as orange arrows and the particle trajectory in dashed red arrows. Figure by Jenni Jormanainen, adapted from Kilpua & Koskinen (2017) and Matthews et al. (2020).

& Uzdensky 2024), but also softer spectra are found in contrast with observations (Comisso & Sironi 2018). Magnetic reconnection is also able to account for the high PD (up to 20%) and PA swings seen in blazars (Zhang et al. 2018). Intra-night-scale variability seen from some blazars poses challenges for shock and stochastic acceleration models because of the small region the emission must originate from. Magnetic reconnection models have been shown to be able to produce variability in such timescales (Giannios et al. 2009; Giannios 2013; Petropoulou et al. 2016), and this was also studied in Paper I by comparing simulated magnetic reconnection scenarios with observations. Finally, it is not known how the jets that are thought to start as magnetically (Poynting flux) dominated flows transform into particle-dominated ones. Magnetic reconnection is an efficient way of dissipating magnetic energy and thus could be the solution to this (Blandford et al. 2017). Magnetic reconnection models are further discussed in Chapter 5.

4 Constraining the jet parameters

The multi-wavelength and -timescale emission of blazars offers various channels to extract information from their jets. Each wavelength has its advantages and disadvantages, and they also probe different regions of the jet. Observations provide clues about the events taking place in the jet environment, and interpretations can be made by modelling different scenarios that could have caused these signatures. In this Chapter, common methods to constrain the jet parameters are introduced and their advantages and caveats are discussed in the context of blazar observations.

4.1 Very long baseline interferometry

The angular resolution of a telescope depends both on the diameter of a dish or a mirror and the observed wavelength, and it can be approximated as $\Theta = \lambda/D$, where λ is the used wavelength and D is the diameter of the dish or the mirror. Therefore, it is possible to increase the observed resolution by decreasing the observed wavelength (i.e. increasing the frequency) or by increasing the size of the dish. In VLBI, antennae separated by great distances act as a single telescope. Increasing the baselines (distances between each antenna) and the frequency simultaneously can offer extremely high spatial resolutions down to sub-milliarcsecond scales. Despite the fact that AGNs are very distant sources, the VLBI technique offers a possibility to image the pc-scale jets in detail (e.g. Piner & Edwards 2004; Piner et al. 2008, 2009; Tiet et al. 2012; Pushkarev et al. 2012; Piner & Edwards 2018). Significant VLBI blazar surveys are the Monitoring of Jets in AGN with VLBA Experiments (MOJAVE[1], see Lister et al. 2019) programme and the monitoring in the Boston University Blazar Group[2] (Jorstad & Marscher 2016), and they offer systematic observations of the apparent superluminal motion in relativistic jets. Latest advances in the VLBI domain include the use of different antennae across the globe with EHT (Event Horizon Telescope Collaboration et al. 2019) and also space-VLBI instruments in which one (or more in the future) antenna is situated in space (Radio-Astron, see Kardashev et al. 2013). Such telescopes offer a great increase in the observed resolution down to microarcsecond scales, probing the regions closest to the SMBH.

[1] https://www.cv.nrao.edu/MOJAVE/

[2] http://www.bu.edu/blazars/BEAM-ME.html

In addition to probing the jet structure, VLBI observations offer different means to estimate the jet parameters. For example, in those sources where superluminal motion of the jet components is seen and tracked over time, the apparent jet speed can be used to calculate the viewing angle and the bulk Lorentz factor of the jet if the Doppler factor has first been derived from observations (through, e.g. assuming equipartition between particles and magnetic field in the emission region, Readhead 1994 and Güijosa & Daly 1996; variability, Lähteenmäki & Valtaoja 1999 and Valtaoja et al. 1999; single-component causality, Jorstad et al. 2005; or brightness temperature, Homan et al. 2021). Bulk Lorentz factor of the jet can be calculated using (see, e.g. Böttcher et al. 2012b)

$$\Gamma = \frac{\beta_{\rm app}^2 + \delta^2 + 1}{2\delta} \tag{20}$$

and the viewing angle using

$$\theta_{\rm obs} = \arctan\left(\frac{2\beta_{\rm app}}{\beta_{\rm app}^2 + \delta^2 - 1}\right), \tag{21}$$

where δ and β are as previously defined in Eq. 1 in Chapter 2.

Through multi-frequency VLBI observations, the positions of the jet components and the radio core can be observed and tracked. Because the radio frequencies are optically thick closer to the SMBH due to synchrotron self-absorption (SSA), the stationary radio core, from which the moving features emanate, is seen shifting from closer to the SMBH in the higher frequencies to further out in the lower frequencies. This means that in the higher frequencies (millimetre wavelengths) the observed radio core likely corresponds to a standing shock within the jet whereas in the lower frequencies (centimetre wavelengths) the core is the surface where the optical depth, τ, becomes smaller than unity (e.g. Daly & Marscher 1988). Those jet regions that only emit in the optically thin wavelengths, meaning that their location does not change as a function of frequency, can be used to align images at different wavelengths. It is then possible to measure the core shift as a function of wavelength, and an estimate of the jet magnetic field can be obtained by assuming that the jet particles and the magnetic field are in equipartition, that is the energy they carry is equal, in the core (Pushkarev et al. 2012). Alternatively, observing the turnover frequency of the synchrotron spectrum for the individual moving components seen in VLBI can be used to estimate the magnetic field strength (Savolainen et al. 2008).

In Paper IV, VLBI imaging results were used to revise the propagation speed for a new moving component that emerged from the millimetre-radio core of OJ 287. The VLBI observations were carried out with Global Millimeter-VLBI Array (GMVA) at 86 GHz by Lico et al. (2022), and the new component ('K') is shown

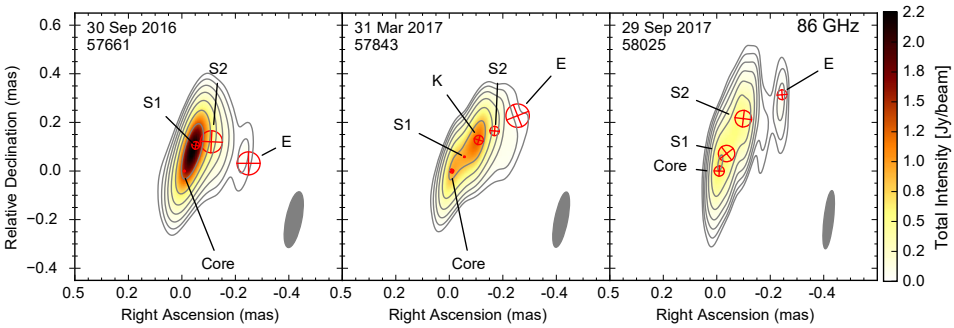

Figure 7. VLBI observations of the pc-scale jet of OJ 287 from Lico et al. (2022) across three observation epochs. The contour lines and the colours describe the total intensity of the jet. The depicted jet components are obtained by modelling the emission with Gaussian components in the visibility plane. The stationary millimetre core is seen left-most in all panels. Quasi-stationary components S1 and S2 are seen in all panels, and in the second panel, a moving component K is detected between them. Figure adapted from Lico et al. (2022).

in Fig. 7 in the second panel between two quasi-stationary features ('S1' and 'S2'). In Paper IV, the revised speed was used to further establish the link between the passage of the moving component through a quasi-stationary jet feature and the first observed VHE gamma-ray flare from the source. In Paper I, the input parameters for magnetic reconnection simulations were derived from literature data, and, for example, the bulk Lorentz factor was estimated using theoretical upper limits from VLBI observations (Piner & Edwards 2018) of the HSP blazar Mrk 421. Similarly, estimations from the VLBI observations were used to justify, for example, the size of the emission region in Paper III.

4.2 Multi-wavelength observations

Multi-wavelength observations of blazars are essential to understand relativistic jets as a whole. They allow recognising quasi-periodicities or patterns from one flaring event to another, although the processes that cause flaring and quiescent states are not yet fully understood. Observations at different wavelengths can be used to identify emission components of the AGN through SED modelling. Variability observations can help to understand the source behaviour in different timescales; short-term intensive campaigns assess fast variability and the emission region sizes, and long-term monitoring, spanning already more than a century for some blazars, can be used to study the connection between emitting regions at different wavelengths. SED modelling and MWL variability are the focus especially in Paper III. In Paper IV, MWL variability is connected with polarisation and VLBI observations.

4.2.1 Spectral energy distribution modelling

As shown in Chapter 1, there are typically two major bumps dominating the SED shape of a blazar. In the lower energies, from radio to X-rays, the emission is attributed to synchrotron emission (Ghisellini et al. 2010) whereas in the higher energies, from X-rays to gamma rays, it is typically thought to result from the IC mechanism (Rees 1967; Maraschi et al. 1992). The observed broadband emission is expected to result from the different emission mechanisms present in the AGN and jet domain, and by modelling the SED, some jet parameters can be estimated (Kirk et al. 1998; Tavecchio et al. 1998).

The simplest SED model of a jet involves a single emitting region, from which all the observed emission stems, and the jet consists of relativistic electron-positron plasma and cold (i.e. subrelativistic) protons. The high-energy emission results from the synchrotron self-Compton (SSC) mechanism with the synchrotron emission providing the seed photons to be upscattered by the relativistic electrons. The advantage of a simple model is having a small number of parameters that characterise it, and such models have been shown to successfully describe those BL Lacs where no external photon fields, such as the dusty torus or the BLR, are seen (Bloom & Marscher 1996; Tavecchio et al. 1998). A typical drawback in the one-zone models is the underestimated radio emission. The emitting regions closer to the SMBH are self-absorbed due to SSA, and because the entire jet is reduced to a single emission region, the low radio frequencies are often not reproduced by these models. Additionally, the properties of some blazars appear to change from one activity state to another (changes during highest activity flares sometimes being especially extreme), requiring more elaborate models. These include for example models with external Compton (EC, e.g. Aleksić et al. 2014b) and models with two emission zones (e.g. Aleksić et al. 2014a; Tavecchio & Ghisellini 2016; Cerruti et al. 2017; MAGIC Collaboration et al. 2020b).

Another important aspect that affects the SED of these sources is the particle composition of the jet which is not exactly known to this day. In many sources, pair-plasma explains the observed features well, but as an alternative, lepto-hadronic models with relativistic hadrons in addition to leptons have been developed. Such models are desirable because the inclusion of relativistic hadrons would mean that blazars are able to produce neutrinos (see Chapter 2). In relativistic jets, hadrons could radiate through proton synchrotron mechanism (Mannheim 1996; Aharonian 2000; Mücke & Protheroe 2001) or photohadronic processes (Aliu et al. 2014; Dermer et al. 2014), the latter of which will also produce neutrinos. Lepto-hadronic models have been shown to explain the observed SED well in some sources (Böttcher et al. 2013; Acciari et al. 2022). However, challenges of lepto-hadronic models are often the high magnetic field strengths required to accelerate the heavier protons and, thus, high jet powers (Cerruti et al. 2019), and the need for dense photon fields

(Waxman & Bahcall 1998; Murase et al. 2014). Originally, hadronic models were developed to suggest blazars as the origin of ultra high-energy cosmic rays (Mannheim 1993). The localisation of cosmic rays is challenging because they are easily deflected by intergalactic magnetic fields, and they have a tendency to interact with the cosmic microwave background through photo-pion production. If hadrons exist in the blazar jets, neutrinos are the more likely signature to prove this because they are not easily affected by external forces. Another observable feature that could differentiate between the pure leptonic and lepto-hadronic models is the 'valley' between the synchrotron and the IC bump that often falls within the X-ray energies. In the hadronic scenario, the valley between the two bumps is flattened due to the synchrotron emission of electrons created in the hadronic cascades. However, this would require a source where it can be appropriately probed with the current X-ray instruments. Finally, X-ray polarisation observations could help solve this conundrum; if the high-energy component was produced by proton synchrotron emission, its PD would have to be as high as that in the low-energy component (Zhang 2017; Liodakis et al. 2019). This could be tested by observing X-ray polarisation from LSP blazars where X-rays are seen as part of the high-energy bump although recent upper limits deem hadronic mechanisms as less likely (Marscher et al. 2024).

The shape of the SED in blazars depends on the activity state of the jet because the jet can hide the emission from the dusty torus or the BLR and push the entire SED to higher energies. Drastic changes can be seen during flaring epochs, and accommodating such changes, for example, by a change in the magnetic field strength or the Doppler factor, within physically reasonable limits is not trivial. Efforts to account for the time evolution of the SED have been made in recent years (Aleksić et al. 2015; Krauß et al. 2016; Lucchini et al. 2019). In paper III, the SED from a flaring epoch was modelled considering the time evolution between four defined activity states. These are shown in the four panels of Fig. 8, the dashed and solid lines representing leptonic and lepto-hadronic models, respectively. The flaring states (A–D) were defined by fitting the VHE gamma-ray SED with either a log-parabola or a power law model. The changes in the broadband SED shape were achieved with minimal, physically justified changes to the jet parameters in both cases.

The parameters that can be constrained through, for example, two-zone SED modelling are the emission region size, R, Doppler factor, δ, magnetic field strength, B, the shape of the electron spectrum (typically described by a broken power law with slopes n_1 and n_1, and minimum, break, and maximum Lorentz factors of the electrons γ_{min}, $\gamma_{\rm b}$, and $\gamma_{\rm max}$, respectively), the electron density, N, and the jet power, $P_{\rm jet}$. In addition to the total jet power, the jet power can be calculated separately for the emitting particle populations and the Poynting flux of the jet. These can, in turn, be used to estimate the equipartition, the ratio between the magnetic and particle energy densities $U_{\rm B}/U_{\rm e}$, of the jet. The ratio $U_{\rm B}/U_{\rm e}$ is also known as the magnetisation parameter typically defined as $\sigma = B^2/4\pi\rho c^2$, where ρ is the density

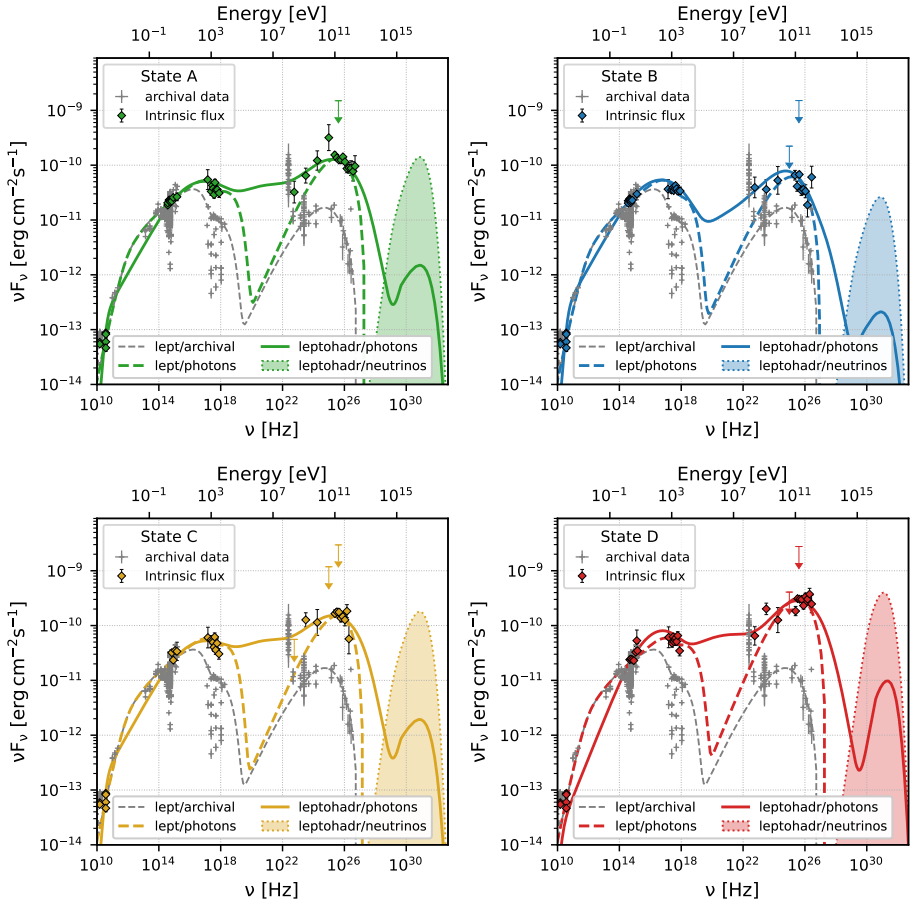

Figure 8. Broadband SEDs of the four flaring states of VER J0521+211 during the VHE gamma-ray flare of 2020. Archival data from MAGIC Collaboration et al. (2020b) are shown in grey while the data of each epoch are shown in their respective colours. The two-zone leptonic model fluxes are shown as dashed lines and those of the one-zone lepto-hadronic model are shown as solid lines. The predicted neutrino spectra from the lepto-hadronic model are shown as dash-dotted lines with filled areas. Figure from Paper III.

of the ions of the cold plasma. The formulae describing δ and B have some degeneracy, and they are typically fixed through other observational constraints before modelling the SED to decrease the number of free parameters. Although SED modelling is a useful tool for estimating these parameters, many leptonic models often result, for example, in a very low B compared to the estimations from VLBI observations. Additionally, the Doppler crisis results exactly from the contrast between the high δ often obtained through SED modelling during flaring epochs and the low jet velocities seen in the VLBI (see Chapter 2). In Paper III, the SED modelling was based on the work of MAGIC Collaboration et al. (2020b), in which the emission region sizes were estimated through VLBI observations and variability timescales.

4.2.2 Variability studies

The observations of the variability patterns in blazars have continued for many decades for some sources (e.g. OJ 287 with optical observations for over a century). Many monitoring programmes (e.g. in optical, Tuorla blazar monitoring[3]: Takalo et al. 2008, Boston University Blazar Group: Jorstad & Marscher 2016, and Steward observatory blazar monitoring[4]: Smith et al. 2009; in radio, Metsähovi at 37 GHz: Teräsranta et al. 1998 and Owens Valley Radio Observatory (OVRO) at 15 GHz: Richards et al. 2011) target specifically blazars and other AGNs, and there are several other telescopes and instruments (e.g. *Swift* X-Ray Telescope (XRT) in X-rays; *Fermi* Large Area Telescope (LAT) in the high-energy (HE, 100 MeV $<$ E $<$ 300 GeV) gamma rays; MAGIC (Major Atmospheric Gamma Imaging Cherenkov), HESS (High Energy Stereoscopic System), VERITAS (Very Energetic Radiation Imaging Telescope Array System) telescopes in VHE gamma rays) that provide long-term data of AGNs among other sources. Comparing the long-term light curves can be used to better understand the emission mechanisms and the regions they originate from.

One way to extract information from the long-term light curves is through the search for periodicities. There are several studies on blazars that are thought to possess quasi-periodic behaviour in their light curves (e.g. Ackermann et al. 2015; Otero-Santos et al. 2020; Sarkar et al. 2021). In the century-long optical light curve of OJ 287, two quasi-periodic signatures have been identified; a 60-year cycle and a 12-year cycle (Sillanpää et al. 1996; Valtonen et al. 2006). The timing of the repeating flares in the shorter cycle has been predicted since the 1980s, and it has typically been connected with various scenarios; a binary SMBH scenario (Sillanpää et al. 1988; Valtonen et al. 2008), jet precession caused by the secondary (Dey et al. 2021), and a wobbling jet (Agudo et al. 2012). However, models that require no binary sys-

[3] https://tuorlablazar.utu.fi/

[4] https://james.as.arizona.edu/~psmith/Fermi/

tem have also been suggested as the explanation of this periodicity (e.g. precession: Liska et al. 2018; Britzen et al. 2018, 2023 and shock-in-jet models: Marscher et al. 2008). For most sources the periodicities break after the observations are continued longer (Hovatta et al. 2008), and this poses one of the biggest challenges when trying to find repeating patterns in blazars which have not been observed for several decades. Variability information alone might not be enough to differentiate between complex models especially because pure red noise process can cause, for example, quiescent states followed by sudden flaring or flaring that appears to repeat (Vaughan et al. 2016; Kankkunen et al. 2025a,b). The stochastic variability process behind the long-term variations can be studied through the power spectral density analysis that can assess the characteristic timescales, that is the timescale that contributes the most in the variability pattern.

The variability in different wavelengths is often correlated (e.g. Acciari et al. 2011; Max-Moerbeck et al. 2014; Aleksić et al. 2015; Lindfors et al. 2016; MAGIC Collaboration et al. 2020a). The connection between the wavelengths is typically studied through cross-correlation. However, cross-correlation can suffer from irregularities in the sampling of the observed data, for example, in the case of those ground-based observations that can be performed only during nighttime, the data can have long gaps. Evenly sampled data sets are rare in astronomical sources in multiple wavebands, and using methods like the discrete correlation function (Edelson & Krolik 1988; Hufnagel & Bregman 1992) can be used to avoid the problems related to the data limitations. Typical studies in the case of blazars search for common patterns or time lags between data sets of different wavelengths. Such studies associate correlated behaviour between emissions with a common, likely co-located origin. In turn, a time lag would indicate a separation between the regions where the two emissions stem from. In Paper III, a cross-correlation analysis was performed and a negative time lag (higher energies leading the lower energies) was found between the optical and radio wavelengths while the variations in the HE gamma rays and optical band were essentially simultaneous. The variability analyses were used to support the leptonic SED model with two separate emission zones.

Estimating the variability timescales in the radio band is especially useful. Through single-dish observations, the flare amplitude and the minimum variability timescale can be used to estimate the brightness temperature of the source, which in turn can be used to calculate the variability Doppler factor. The variability timescale is often obtained through a decomposition of the flares within the light curve, and typical decomposition methods include, for example, exponential fitting (e.g. Valtaoja et al. 1999; Hovatta et al. 2009) and Bayesian blocks (Scargle 1998; Scargle et al. 2013). With the observed flare amplitude, $\Delta S_{\rm max}$, and variability timescale, $t_{\rm var}$, the observed brightness temperature, $T_{\rm b,var}$, can be obtained using (see Eqs. 2 and 3 in Hovatta et al. 2009)

$$T_{\rm b,var} = 1.548 \times 10^{-32} \frac{\Delta S_{\rm max} d_L^2}{\nu^2 t_{\rm var}^2 (1+z)}, \tag{22}$$

where d_L is the luminosity distance of the source, ν is the observing frequency, and z the redshift of the source. Then the variability Doppler factor can be calculated using

$$\delta_{\rm var} = \left(\frac{T_{\rm b,var}}{T_{\rm b,int}} \right)^{1/3}, \tag{23}$$

where $T_{\rm b,int}$ is the intrinsic brightness temperature of the source, and it is typically assumed to be the equipartition temperature $\sim 10^{11}$ K (Readhead 1994; Lähteenmäki et al. 1999).

The short (hour-to-minute) timescale variability in the optical-to-HE-gamma-rays is a phenomenon common to blazars because of their Doppler-boosted jet emission. The most extreme variations appear in the VHE gamma rays and have been seen from a handful of blazars (e.g. in Mrk 421: Gaidos et al. 1996, Mrk 501: Albert et al. 2007, PKS 2155−304: Aharonian et al. 2007, PKS 1222+21: Aleksić et al. 2011, BL Lac: Arlen et al. 2013) but also from a radio galaxy (IC 310: Aleksić et al. 2014c). The size of the emission region can be calculated from the variability timescale $\Delta t_{\rm var}$ as (see, e.g. Böttcher et al. 2012c)

$$R \leq c\, \Delta t_{\rm var}\, \delta. \tag{24}$$

In the case of the fastest variability timescales observed from the sources mentioned above, a ∼2-minute variability timescale would mean that with the typical $\delta \sim 10$, the emission region size is of the order 10^{13} cm, or 3×10^{-6} pc, which is an extremely compact region compared to the typical jet cross-sections of $\sim 3 \times 10^{-2}$ pc (at 0.05 pc from the SMBH and assuming an opening angle of ∼2° Pushkarev et al. 2017) or the size of the event horizon $\sim 2 \times 10^{-4}$ pc (a SMBH with $M = 10^9 M_\odot$). Therefore, observing the minimum variability timescales at each wavelength can be used to derive the sizes of their respective emission regions, and it can also give hints about the co-location of these emissions, although simultaneous MWL observations of intranight variability are rare (Zacharias et al. 2017; Acciari et al. 2020).

Fast variability was especially in focus in Paper I, in which the fast VHE gamma-ray flares seen from the HSP BL Lac Mrk 421 were suggested to be explained by magnetic reconnection (further discussed in Chapter 5). Multi-wavelength variability information can also offer further context for other data. For example, the long-term data used in Paper III were compared with the data from the flaring epoch, and in Paper IV, optical and MWL radio flux densities were compared with polarisation data (see Fig. 9).

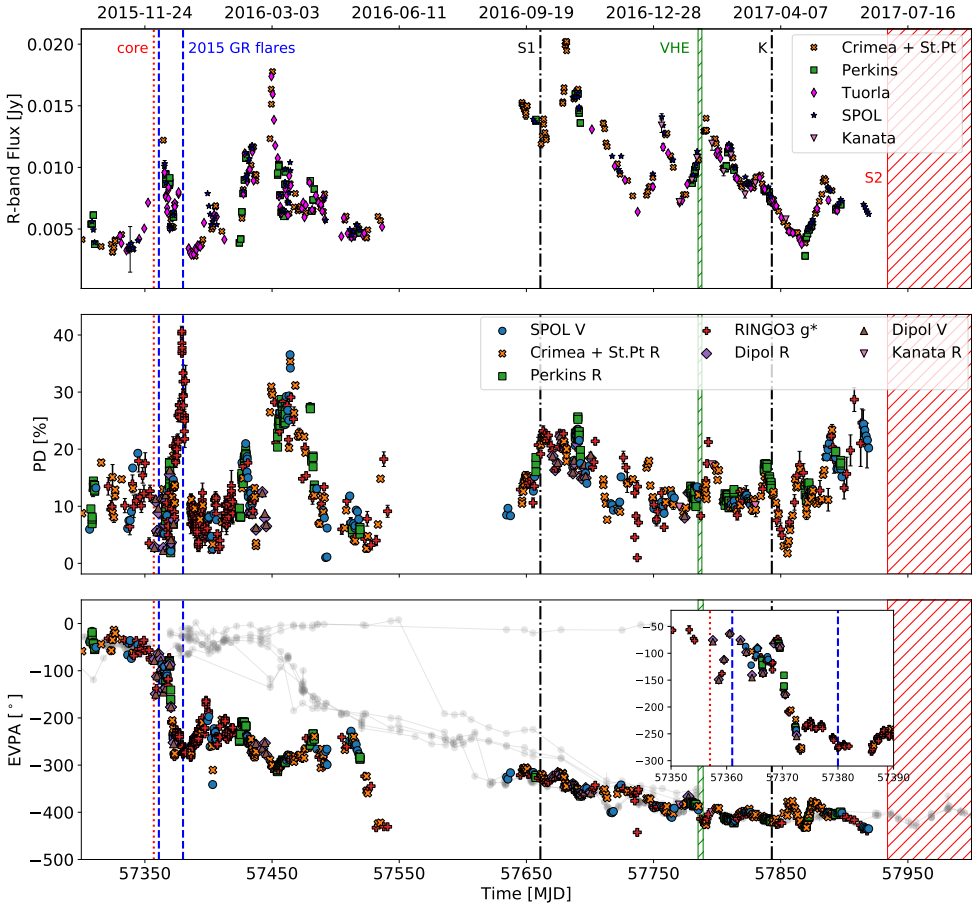

Figure 9. Light curves displaying the *R*-band flux and combined *R*-, *V*- and *g**-band PD and PA curves. Notice that in the bottom panel, PA is abbreviated as 'EVPA' as in 'electric vector position angle'. The inset panel shows a zoomed-in view of the long rotation seen in the optical data. The grey data points in the bottom panel show the evolution of the various radio bands. The vertical dashed blue lines mark the times of the optical flares predicted by the binary SMBH model (Valtonen et al. 2016). The vertical dot-dashed black lines mark the 86 GHz GMVA epochs when quasi-stationary feature S1 was seen brightened and when the moving component K was detected (see Fig. 7, and Lico et al. 2022). The green hatched area marks the period of VHE flaring (Acharyya et al. 2024). The vertical dotted red line marks the time when K should have still been residing within the millimetre-radio band core, and the red hatched area is the estimated time when K reached quasi-stationary feature S2. Figure from Paper IV.

4.3 Polarisation

As discussed earlier, synchrotron emission is inherently polarised due to the electrons gyrating in the magnetic field of the jet, thus, polarisation traces the magnetic field itself. Like their flux densities, the polarisation in blazars varies on diverse timescales all the way down to intra-night scales. Observations and modelling of polarisation from relativistic jets are useful to extract information about the projected magnetic field of the jet, the acceleration mechanisms, as well as the launching and collimation of the jet.

Polarised light is often described with the Stokes parameters: I, that is the total intensity of the light, Q and U give the components of the linearly polarised wave, and V describes circular polarisation. Using the Stokes parameters, the degree of linearly polarised intensity can be calculated as (see, e.g. Nilsson et al. 2009)

$$\mathrm{PD} = \frac{\sqrt{Q^2 + U^2}}{I}, \tag{25}$$

and the electric vector position angle is given by

$$\mathrm{PA} = \frac{1}{2}\arctan\left(\frac{U}{Q}\right). \tag{26}$$

Linear polarisation can be observed from relativistic jets in wavelengths from radio to optical, and more recently also in X-rays thanks to the Imaging X-ray Polarimetry Explorer satellite (IXPE, Weisskopf et al. 2022). Blazars are known for their high PDs typically reaching 10–20%, sometimes even up to 40–50% (Scarpa & Falomo 1997; Morozova et al. 2014; Angelakis et al. 2016; Smith 2017). Variability of the PD can be interpreted as the changes in the magnetic field of the jet (ordering of the magnetic field gives high PDs, turbulent field low PDs) and as different emission mechanisms (e.g. thermal emission unpolarised, synchrotron emission polarised). Polarisation signatures of blazars have successfully been explained with shock models in the past (Hughes et al. 1985, 1989a,b; Aller et al. 2014). Because shocks order the magnetic field, they are able to produce even the high observed PDs (Marscher & Gear 1985; Hughes et al. 1985).

The rotations of PA are often defined as those events, where the PA changes at least 90° with the difference between subsequent data points remaining smaller than 90° (Kiehlmann et al. 2021). Such rotations or polarisation angle swings are typical for many blazars (Blinov et al. 2016), and fast PA swings or rotations of hundreds of degrees have been observed for some sources (Marscher et al. 2008; Marscher et al. 2010; MAGIC Collaboration et al. 2018). Additionally, rotations can be traced using the Stokes parameters Q and U since any visible rotations in the PA should

be a result of a loop around the origin in the Q–U plane. Sometimes these loops can lie outside the origin, in which case they do not appear as visible PA rotations. Such hidden rotations can still be used to understand differences, for example, in the polarisation behaviour of different wavelengths (Cohen & Savolainen 2020; Blinov et al. 2021). There is also evidence that gamma-ray flares often occur simultaneously with PA rotations (Marscher et al. 2010; Abdo et al. 2010b; Pavlidou et al. 2014; Blinov et al. 2018), implying a connection between magnetic fields and flaring in the higher energies. In addition to the variable behaviour, many blazars appear to have stable, preferred PAs over long periods of time (Angel et al. 1978; Hagen-Thorn 1980; Jannuzi et al. 1994; Villforth et al. 2010; Hovatta et al. 2016). This in turn supports a multi-component model where the jet likely has a stable polarised component, on top of which chaotic bursts are seen producing variations (Bjornsson 1982; Cohen & Savolainen 2020).

Polarisation of light can be altered by some magnetised medium, typically called a screen, between the source and the observer. This effect is known as Faraday rotation, and due to its wavelength dependency, it can be particularly prominent in the observed PAs in radio wavelengths. In blazars, Faraday rotation can be used to study the intrinsic magnetic fields in the jet and its plasma properties because Faraday rotation is also dependent on the electron density of the plasma. The morphology of the magnetic field can be further studied by observing a gradient of the Faraday rotation within the pc-scale jet using VLBI observations. Such observations have found evidence of toroidal magnetic field components, hinting at the existence of a sheath structure in the jet (Asada et al. 2002; Zavala & Taylor 2005; Hovatta et al. 2012).

The synchrotron emission from blazars is also expected to be circularly polarised, but the fractions are typically much lower than in the linear polarisation (Valtaoja et al. 1993; Wagner & Mannheim 2001; Homan & Wardle 2004; Homan & Lister 2006; Hutsemékers et al. 2010; Liodakis et al. 2022, 2023). Circular polarisation can be used to estimate the minimum Lorentz factor of the electron distribution, $\gamma_{\rm min}$, by studying the low-energy particles whose linear polarisation degree may be converted into circular in Faraday conversion when these particles traverse down the jet (e.g. Beckert & Falcke 2002).

Polarisation data were analysed in three papers included in this thesis. In Paper II, the X-ray polarisation observations with the IXPE satellite along with optical and radio polarisation were used to seek evidence for the dominant acceleration mechanism of the jet in the HSP blazar Mrk 501. The MWL polarisation results were evaluated against the expectations of four different models. The MWL polarisation was observed to be strongly chromatic, meaning that the PD in X-rays was observed to be higher than that in the optical and radio wavelengths. This is demonstrated in the left panel of Fig. 10. The observed and the expected PD ratios between optical and X-rays are compared on the right panel. The variability in the X-ray polarisation

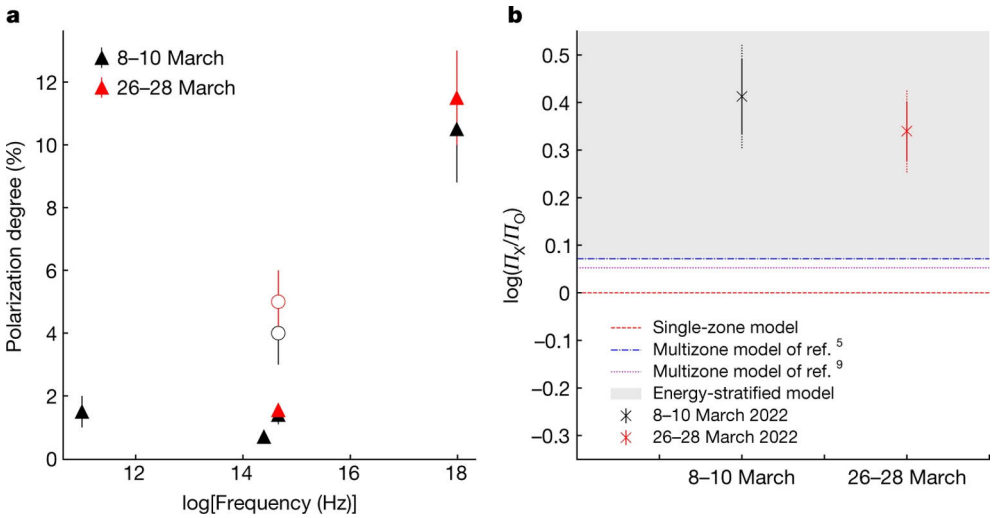

Figure 10. Measured MWL polarisation of Mrk 501. On the left: PD from radio to X-rays from two different observation epochs. The open symbols show the intrinsic optical PD, corrected for the unpolarised light contribution from the host galaxy. On the right: Comparison between the observed logarithm of the X-ray and optical PD ratio and the expectations from various models. Figure from Paper II.

was detected to be slow, and the PA was observed to be aligned with the jet axis. These signatures together were interpreted as evidence that the magnetic field in the emitting region must have been ordered and that the emission in the X-rays originates closer to this region. This implies that the dominant acceleration mechanism in this jet region is shock acceleration.

The long-term polarisation signatures of the blazar VER J0521+211 were modelled in Paper III using a two-component model with a stable jet component ('core') and three burst components ('spheres') with Gaussian density profiles. The polarisation model used the results of the SED modelling performed in the same study to fix some parameters of the model, namely δ, B, and R. In the model, the burst components are set to pass through the core, and the polarisation is measured solely within the core region. The changes in the polarisation are then a result of disturbances in the electron density of the core. The observed polarisation signatures were only partly reproduced by this simple model, and this was taken as evidence that the jet conditions at the time of the VHE flare must have differed from those in earlier epochs. Additionally, more sophisticated models, for example, with contributions from several polarised components or with components that are physically rotating in the jet magnetic field might be needed to create the fast PA swings seen in the polarisation data.

In Paper IV, optical and radio polarisation data of OJ 287 were evaluated in the context of various observed events between 2015 and 2017. Additional millimetre-

band data from the AMAPOLA[5](Analytic Matrix for ALMA POLArimetry) monitoring programme (Kameno 2023), and optical polarisation data from several telescopes were used to refine the model suggested by Myserlis et al. (2018), and to explain the polarisation signatures from this period. The optical data was used to sketch out a scenario where the onset of a new moving component in the jet of OJ 287 was seen as a long PA rotation (see the bottom panel and the inset of Fig. 9). This moving component was later detected in VLBI observations by Lico et al. (2022) who connected it with the first VHE flare of OJ 287. Additionally, the millimetre bands that initially followed the centimetre bands were later seen to follow the optical PA more closely, indicating a change in the jet opacity between different wavelengths. This transition was seen simultaneously with the moving component passing a quasi-stationary feature seen in the VLBI observations.

[5] https://www.alma.cl/~skameno/AMAPOLA/

5 Simulating fast variability

The mechanism behind the short timescale variability, especially in the VHE gamma rays where the fastest minute-scale flares are seen, is not fully understood. As explained in Chapter 4.2.2, the derived minimum timescales of the fastest flares (e.g. Aleksić et al. 2014c; Abeysekara et al. 2018; Acciari et al. 2020) imply that the emission region must be much smaller than the size of the event horizon in these sources. Additionally, very high Doppler factors (order of $\delta \sim 50$) are required for the TeV photons to avoid self-absorption in that emission region. Such requirements pose challenges for the acceleration mechanism and the emission region. Various scenarios that could produce variability on such short timescales have been suggested (Ghisellini & Tavecchio 2008; Lyutikov & Lister 2010; Narayan & Piran 2012; Barkov et al. 2012), but perhaps the most convincing mechanism is magnetic reconnection (Giannios et al. 2009; Giannios 2013). The presence of magnetic reconnection in the relativistic jets could be expected because they are thought to be launched as Poynting flux-dominated flows but are later thought to convert to particle-dominated ones through some mechanism (see Chapter 2). In this Chapter, simulations of magnetic reconnection in the blazar jets are briefly introduced. In addition, the magnetic reconnection model used in Paper I is described, and the methodology to produce the simulations, the comparison work, and its results are summarised. Finally, some future remarks are discussed.

Simulations of magnetic reconnection are two kinds; kinetic particle-in-cell (PIC, e.g. Kagan et al. 2015; Guo et al. 2019, 2023; Comisso & Sironi 2019; Zhang et al. 2021, 2023; Chernoglazov et al. 2023) and MHD simulations (e.g. Kowal et al. 2011; de Gouveia Dal Pino & Kowal 2015; del Valle et al. 2016; Kadowaki et al. 2021; Medina-Torrejón et al. 2021, 2023). The differences between these are that the MHD simulations are driven by turbulence and focus on the large, astrophysical scales whereas the PIC simulations are driven by tearing instabilities and often probe the microscopic scales of the plasma. Recent applications of PIC simulations to long temporal and spatial scales have, however, proven promising and showed that they are capable of accelerating particles to the highest energies seen from blazars (Sironi & Spitkovsky 2014; Sironi et al. 2015, 2016; Petropoulou et al. 2016). The advantage of the large-scale PIC simulations is their capability to produce simulated light curves, allowing a direct comparison of the simulated data with observations. The magnetic reconnection model based on the work of (Sironi et al. 2015, 2016;

Petropoulou et al. 2016; Christie et al. 2019) was used in Paper I to perform such a comparison.

The short timescale variability in blazar jets is often suggested to be related to quasi-spherical blobs called plasmoids, each with relativistic particles and magnetic fields, emanating within the jet (Mastichiadis & Kirk 1995; Bloom & Marscher 1996; Chiaberge et al. 1999; Celotti & Ghisellini 2008). Magnetic reconnection is able to produce plasmoids when a current sheet, a plasma surface between two magnetic fields of opposite direction, forms in the jet (Spruit et al. 2001; Giannios & Spruit 2006; Barniol Duran et al. 2017; Gill et al. 2018), and is disrupted into magnetic islands, a chain of plasmoids, due to intrinsic tearing instabilities in the jet plasma (Loureiro et al. 2007; Fermo et al. 2010; Uzdensky et al. 2010; Huang & Bhattacharjee 2012; Loureiro et al. 2012; Takamoto 2013). In this scenario, the reconnection layer acts as a mini-jet, a subregion within the jet, that can have a different orientation to that of the pc-scale jet. This corresponds to the jet-in-jet model suggested by Giannios (2013).

Blazar jets are expected to be in equipartition, $U_{\rm B}$ being roughly equal to $U_{\rm e}$ (e.g. Komissarov et al. 2007, 2009; Tchekhovskoy et al. 2009; Vlahakis 2015). This is also inferred from comparing the jet and the accretion power (Ghisellini et al. 2010, 2014) and the observations of brightness temperature in radio (Readhead 1994; Lähteenmäki et al. 1999; Homan et al. 2006; Hovatta et al. 2013). Some mechanism is needed to dissipate the initial magnetic energy of the jet. While shocks could be the solution, it is known that the formation of shocks and their efficiency to accelerate particles is diminished in strongly magnetised flows (Kennel & Coroniti 1984; Giannios et al. 2008; Narayan et al. 2011). Sironi et al. (2015) showed that magnetic reconnection is able to efficiently dissipate the magnetic energy of the initially Poynting flux-dominated jet into particle acceleration. Their two-dimensional (2D) PIC simulations were able to produce an extended non-thermal distribution of relativistic particles as well as plasmoids that could be the origin of the observed variability signatures. In Sironi et al. (2016), this work was continued via large-scale 2D PIC simulations that also tracked all three components of velocities and electromagnetic fields. The simulations were computed for three values of the jet magnetisation σ. After the initial reconnection, the long-term evolution of the plasmoids was tracked as they grew through mergers and accelerated until leaving the reconnection layer. The properties of the plasmoids, such as their speeds and sizes, were recorded for each value of σ.

Petropoulou et al. (2016) combined the results of the 2D PIC simulations of Sironi et al. (2016) with the kinetic equation for the evolution of the distribution of radiating particles as well as their synchrotron and SSC emission. They also calculated the basic properties, rise times and amplitudes, of the flares produced by the plasmoids and found that the largest plasmoids were responsible for the hour-scale variations while the smallest and fastest plasmoids produced minute-scale flares. These

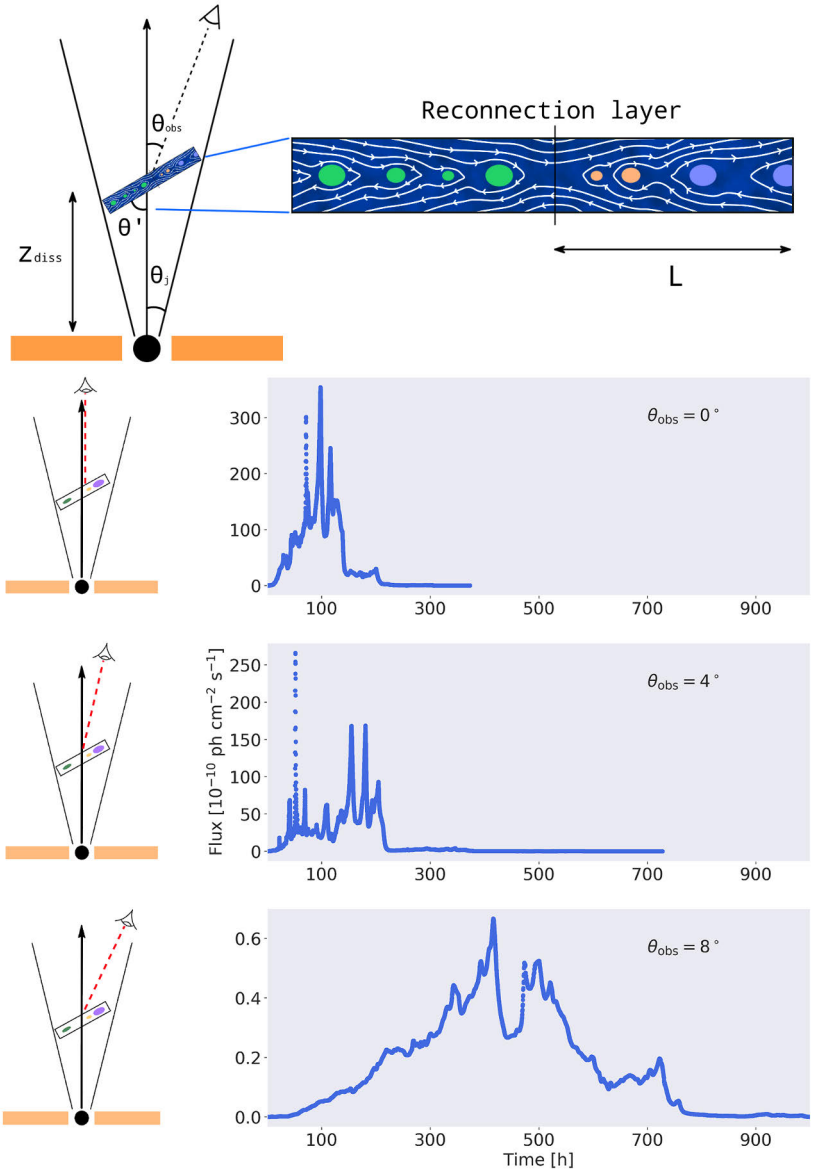

Figure 11. Model of a jet with a current sheet fragmented into plasmoids. Top: The jet seen by the observer at angle $\theta_{\rm obs}$ has an opening angle $\theta_{\rm j}$. The reconnection layer with half-length L is aligned with angle θ' with regards to the jet axis and is situated at a distance $z_{\rm diss}$ from the accretion disc. The plasmoids have different sizes and speeds (orange and blue), those in green are moving away from the observer. Three bottom panels: The observed flux amplitudes and flare durations of the simulated light curve change with varying $\theta_{\rm obs}$. Notice the different y-axis of each light curve. The example light curves are for simulations with $B = 0.1$ G and $\theta' = 50°$. Figure by Jenni Jormanainen, adapted from Christie et al. (2019) and Paper I.

results were further utilised in Christie et al. (2019) whose radiative transfer model was used to track the particle distribution evolution of each plasmoid and to produce their photon spectra. The considered processes in producing the plasmoid spectra were synchrotron emission and SSA, IC scattering in the Thomson (low-energy photons) and Klein-Nishina (high-energy photons) regimes via either SSC or EC with seed photons from the BLR, γ-γ pair production, and photon escape. The individual plasmoid spectra computed in the plasmoid co-moving frames were then combined into the spectrum of the entire plasmoid chain and mapped to the frame of the observer. Christie et al. (2019) successfully showed that this magnetic reconnection scenario can describe the typical broadband spectra of both BL Lacs and FSRQs.

In Paper I, utilising the model introduced in Christie et al. (2019), a comparison between the simulated and observed light curves was performed for one blazar. The HSP BL Lac Mrk 421 was observed with the MAGIC and the VERITAS telescopes in the VHE gamma rays when the source was flaring in 2013 (Acciari et al. 2020). The jet model showing the reconnection layer lying at a distance $z_{\rm diss}$ from the accretion disc and aligned at an angle θ' with regards to the jet axis is depicted in Fig. 11. The simulations were set up by collecting available observed parameters such as the jet power, $P_{\rm jet}$, and synchrotron peak frequency, $\nu_{\rm peak}$, while Γ, $\theta_{\rm obs}$, and B were estimated based on the generally known properties of blazars. The preliminary tests performed in Jormanainen et al. (2021) showed that the initial choice for the jet bulk Lorentz factor that had been derived for sources with no detected apparent velocities via VLBI observations (Piner & Edwards 2018) resulted in fluxes that were 100–1000 times lower than the observed fluxes. Therefore, Γ was multiplied by a factor of three to obtain fluxes that match the observed level. By varying B between 0.1–10 G, $\theta_{\rm obs}$ between 0–8°, and the angle of the reconnection layer between 0–180°, the simulations comprised an array of 285 realisations. The produced light curves were compared with the observed light curves using statistical tests that evaluated the flux amplitudes and variability timescales of the flaring patterns. The results of Paper I showed that those reconnection layer angles that produced a moderate Doppler boosting in combination with the jet viewing angles of 6–8° best matched the observations. This result was also suggested as evidence for solving the Doppler crisis; a reconnection layer with a higher Γ can be aligned in a way that produces high enough Doppler boosting to produce the VHE variability as opposed to the slow or stationary jet component speeds seen in the VLBI imaging of Mrk 421.

5.1 Future studies

Paper I showed that magnetic reconnection can produce variability similar to that seen in VHE flares of blazars. However, there are still several details that require refining work in the future.

The broadband spectra of blazars in the case of BL Lacs show equal synchrotron

and Compton ratios and, in the case of FSRQs, higher Compton dominance. The simulated SEDs through magnetic reconnection used in Paper I originally produced Compton ratios much lower than those seen in the observations of Mrk 421. This was addressed in Paper I by scaling the IC bump with a predetermined factor for the jet energy densities. The possible caveats in the observations, which could be used to compensate for this, were identified in this study, but at the same time, it shows that to achieve high energies in the magnetic reconnection scenario a strong seed photon field is needed. Christie et al. (2020) suggested that larger plasmoids in the reconnection layer could act as an additional source of seed photons in the absence of an external field such as a torus or the BLR. It is also possible that other current sheets exist in the reconnection region. These layers could be misaligned with respect to the observer in a way that the emission from such layers is not visible, but it is enough to provide seed photons for the target layer. Additionally, the spectra from Mrk 421 from this time (Acciari et al. 2019) show significantly harder behaviour than what was achieved in this study. Similar to the low Compton ratios, external photon fields even in BL Lac sources could be used to harden the spectra to match those seen from these sources during flaring. Exploring the external photon fields is left for future studies.

In the case of Mrk 421, the simulated light curves were roughly matched with the observed flux levels. In future work, it would be interesting to try to compare also the SEDs, in addition to the light curves, produced by the simulations and include MWL data. In the case of Mrk 421, simultaneous X-ray data exists from the time of the observational campaign that could be used to determine the shape of the higher energy component in more detail. It would be similarly valuable if simultaneous observations were performed in the optical and VHE gamma-ray bands since also optical intra-night variability is sometimes seen from blazars. Optical polarisation observations together with the VHE gamma-ray data could further be used to evaluate the acceleration mechanism behind such fast variations. The simulations used in Paper I do not have the polarisation properties of the plasmoids included, but PIC simulations combined with radiative cooling and polarized radiation transfer simulations have shown that reconnection could produce variable polarisation and be able to account for the long PA rotations seen in some blazars (Zhang et al. 2018).

Finally, magnetic reconnection is a stochastic process, meaning that the resulting variability signatures are expected to be related to the properties of the generated plasmoids in a given simulation. The 2D PIC simulation results by Sironi et al. (2016) offer only one realisation to test the capabilities of reconnection-induced variability, but if a new set of plasmoids was generated, the produced variability patterns could be different. An alternative way to account for the stochasticity would be to estimate the spectral slope of simulated magnetic reconnection light curves through a power spectral density analysis. The spectral slope could then be used to generate several light curves with the same statistical properties as the original simulation,

introducing an additional statistical layer when analysing flare patterns.

6 Summary of the publications

Active galactic nuclei are some of the most extreme phenomena in the Universe, revealing the immense scale, in which these cosmic engines can affect the surrounding host galaxy and even the neighbouring galaxies. Relativistic jets launched by a fraction of AGNs are one form of such feedback. They are best observed in blazars, in which the jet is pointing almost directly towards us. In these cases, the jet emission drowns most of the emission of the nucleus and the host galaxy, making them excellent sources for studying the jet properties. Yet many questions remain: What mechanisms accelerate particles in the jet, and what causes the fastest variability in the VHE gamma rays? What is the jet magnetic field strength and structure, and what is its role in the jet launching and collimation? What is the particle composition of the jet, and are blazars able to produce neutrinos? This thesis focusses on the first two questions and discusses several methods used in Papers II, III, and IV to analyse and model MWL data from these objects. Another avenue to understand these sources is explored in Paper I through simulations of relativistic magnetic reconnection that are compared with observed VHE gamma-ray light curves. The third question is touched upon in Paper III where two SED modelling scenarios are tested.

The papers included in this thesis attempt to understand the structure of the jet or the acceleration mechanisms in one way or the other. In Paper II, shock acceleration was favoured based on the MWL polarisation signatures observed from Mrk 501, but it appears likely that this mechanism is not able to account for such fast variations as those seen in the VHE gamma-ray range. It is not known exactly where the highest energy emission, especially that which varies on the minute timescales, originates from. It has been suggested that it could be generated in the wake of moving components passing through shocked regions (such as was suggested in the MAGIC Collaboration et al. 2018 and also studied in Paper IV). This could be due to magnetic reconnection in the turbulent downstream regions, but simulations also show that the relativistic magnetic reconnection is likely to be inefficient in particle-dominated environments and in the presence of shocks (Sironi et al. 2015). Conversely, particle acceleration in shocks might be diminished in strongly magnetised environments (Kennel & Coroniti 1984). This would mean that if the fast VHE gamma-ray flares are produced by magnetic reconnection, they would have to originate closer to the jet base than where the standing shocks are seen in the VLBI imaging. However, in sources with external photon fields, γ-γ absorption might prevent us from seeing the

highest energy emission unless it originates near the outer regions of these photon fields (Böttcher & Els 2016).

It is still clear from the observations of the fastest variations that the jet must have smaller subregions where such emission can originate. In Paper I, a solution to the Doppler crisis was suggested in the form of the favourably aligned reconnection layers that are able to produce faster variations in the VHE gamma-ray band than what is suggested by the jet speeds observed with VLBI in radio. In SED modelling, it is often assumed that there exists a smaller region where the higher energy emission originates from, and this was also done in Paper III. This could also be the explanation for the question of whether both shocks and magnetic reconnection can be present in the jet if reconnection dominates the particle acceleration in the magnetised jet base and shocks downstream in the particle-dominated regions. Additionally, some sources sometimes show sub-hour variability in the optical band. In Paper III, the optical emission originates partly from the blob and partly from the core component. Therefore, it would be interesting to explore the capabilities of the magnetic reconnection simulations to produce fast variability in the optical wavelengths. In Paper II, the optical PD was seen to be lower than that measured in the X-rays, and this was expected if the optical emission originates further away from the shocked region.

This chapter summarises the results of each paper included in this thesis.

6.1 Fast variability from magnetic reconnection

In Paper I, simulated light curves produced using a magnetic reconnection model by Christie et al. (2019) were compared with the fast very high-energy gamma-ray flares observed from the HSP BL Lac Mrk 421. The data consisted of observations with the MAGIC and the VERITAS telescopes at three energy ranges between 200–800 GeV during nine consecutive nights in April 2013. The simulations were set up using literature estimates for the jet power, $P_{\rm jet}$, bulk Lorentz factor, Γ, peak frequency of the synchrotron spectrum, $\nu_{\rm peak}$, magnetisation of the jet plasma, σ, and minimum Lorentz factor of the injected particle distribution, $\gamma_{\rm min}$. By varying the magnetic field strength, B, viewing angle, $\theta_{\rm obs}$, and reconnection layer angle, θ', 285 different light curves were obtained.

A statistical methodology was developed to analyse the similarity between the simulations and the observed data. The compared properties included variability timescales, flux amplitudes, and spectral slopes. The comparison of the spectral slopes showed that the observed VHE gamma-ray spectrum was not reproduced in the higher energies. The tests comparing the timescales and flux amplitudes restricted the jet parameters in different ways, with the flux distributions of the light curves providing the narrowest matching parameter space, thus being the most restrictive in this regard. The results of each test were used to determine the final

sample of the best-matching simulations.

The analysis found that the simulations that best match the observed data had $B = 0.1$ G and $\theta_{\rm obs} = 6$–8°, suggesting values of B in line with typical estimations from SED modelling and $\theta_{\rm obs}$ slightly larger than those of most blazars. Additionally, the preferred $\theta' = 60$–70°, 100°, and 140° were aligned in a way that the maximum observed Doppler factors were between 10–25, offering an explanation to the Doppler crisis, a discrepancy between the Doppler factors derived for high and low energies, that is typical for many HSP blazars.

6.2 Multi-wavelength polarisation from shocks

In Paper II, the polarisation observations of the HSP blazar Mrk 501 in X-rays, optical, and radio bands were analysed against the expectations of various particle acceleration models. The polarisation observations in the X-rays became available with the IXPE satellite, and the MWL data were obtained during two campaigns in March 2022. The millimetre-radio data were obtained with the Institut de Radioastronomie Millimetrique (IRAM) telescope at 86.24 and 230 GHz as part of the Polarimetric Monitoring of AGN at Millimeter Wavelengths (POLAMI) programme. The radio observations were only performed during the first campaign. The optical data during both campaigns were obtained using several facilities; the Nordic Optical Telescope (NOT), Haleakala Observatory, the Calar Alto Observatory, Sierra Nevada Observatory, the AZT-8 telescope of the Crimean Astrophysical Observatory, and LX-200 telescope of the St. Petersburg State University. Additional archival optical flux and polarisation and X-ray flux data were collected to examine the long-term behaviour of the source.

The measured X-ray PA during both campaigns ($134 \pm 5^\circ$ and $115 \pm 4^\circ$, respectively) was seen to be aligned with the position angle of the jet which has been determined from VLBI observations ($120 \pm 12^\circ$). No significant variability was detected in the X-ray polarisation between the two campaigns. Finally, the PDs of each wavelength were compared, and the PDs in the X-rays were seen to be significantly higher (10 ± 2 and $11 \pm 2\%$, respectively) than those in the radio ($1.5 \pm 0.5\%$ during only the first campaign) and optical bands ($4 \pm 1\%$ and $5 \pm 1\%$, during the first and second campaign).

The comparison of the results between the different models reveals the model that best fits the particle acceleration scenario of the source. The tested models were single-zone, multi-zone, energy stratified (shock), and magnetic reconnection through the kink instability model. The observed signatures: the strongly chromatic MWL PD, slow X-ray polarisation variability, and the X-ray PA along the jet axis, correspond to the energy-stratified shock model. These signatures are expected from this model because the polarisation in the X-rays is assumed to originate near the shocked region whereas in the lower energies, it is emitted further out. The ordering

of the magnetic field in shocks essentially means that the variability of the polarisation in shocks is slow in the higher energies closer to the ordered regions versus the more turbulent downstream. The ordering of the helical magnetic field also means that the PA of the higher energies is expected to be aligned with the jet because the direction of the magnetic field in that region is perpendicular to the jet direction.

6.3 Time-dependent spectral energy distribution modelling

In Paper III, the spectral energy distribution of the blazar VER J0521+211 was modelled from the time of a VHE flare observed with the MAGIC telescopes. Multiwavelength data were collected from the time of the flare (six consecutive nights in February – March 2020) as well as from an extended period (September 2009 – March 2021) to analyse the long-term behaviour of the source.

The variability behaviour of the source was determined to be different during the 2020 VHE flare with flaring observed only in the energies above X-rays, whereas an earlier VHE gamma-ray detection in 2013 showed simultaneous variability in all energies. The long-term variability was further evaluated with a cross-correlation analysis using a discrete correlation function method (Edelson & Krolik 1988). Correlation was tested between radio–optical, radio–HE gamma rays and optical–HE gamma rays. Time lags of -160 ± 11, -140 ± 13 and 20 ± 12 days were found, respectively, with negative time lag implying that the higher energy leads the lower energy and vice versa. This was interpreted as evidence that the radio and optical emissions have a common origin, but their emission regions are likely not entirely co-spatial.

The HE and VHE gamma-ray spectra were modelled to estimate the redshift of the source. A profile likelihood was constructed for three different estimations of instrumental calibration uncertainties, and a 95% upper limit of $z \lesssim 0.244$ was obtained.

The short-term VHE gamma-ray data was used to estimate four different activity states for the 2020 flare. The SED was modelled using a non-interacting two-zone leptonic model and a one-zone lepto-hadronic one for each of the four states. The modelling parameters were first limited to archival observational estimates from MAGIC Collaboration et al. (2020b), and only minor changes in the magnetic field strength, the shape of the electron and proton spectra, and the electron density were allowed between the four different emission states. Both models successfully reproduced the observed features.

Finally, the long-term optical polarisation was modelled using a simple cylindrical jet where the variations of the intensity and the polarisation stemmed from changes of density in the emission region. The results of the leptonic SED modelling were used to fix the Doppler factor, δ, magnetic field strength, B, and emission region

radius, R, in the polarisation model. The polarisation variability closer to the 2020 flare was well reproduced by the polarisation model. However, the data around the earlier 2013 flare were not fitted by the same parameters. Moreover, the PA showed large swings that were not reproduced by the simple cylindrical jet model and were suggested to require a more complex model.

6.4 Polarisation behaviour of OJ 287

In Paper IV, the optical, millimetre, and radio polarisation behaviour of OJ 287 was studied in the context of several observed events between October 2015 and September 2017. The collected data included centimetre-radio data from Myserlis et al. (2018) who reported a long PA rotation at 8.35 and 10.45 GHz. Additional optical data from several telescopes and millimetre-band data from the AMAPOLA monitoring programme were collected to be included in this study.

The analysis of the optical polarisation data revealed a fast 210° PA rotation and several smaller rotations on top of a longer, moderate rotational behaviour. This fast rotation was observed about a hundred days prior to the long PA rotation in the centimetre bands. The added millimetre-band PA data are seen to follow the centimetre data closely until a later epoch where the PA starts to show more structure, following the optical behaviour. In all bands, similar rotation rates between -0.6 to $-0.8^\circ/\mathrm{day}$ are seen until April 2017 when the PA in all bands stabilises.

Lico et al. (2022) presented the VLBI observations of the OJ 287 jet observed with the GMVA at 86 GHz, in which a new moving component ('K') was seen between two quasi-stationary jet features. In Paper IV, the VLBI results were used to revise the speed for K to a 0.12 mas/yr. This speed was then used to calculate the time when K must have still been inside the millimetre core. The multi-band radio spectra were examined from this time, and the emergence of K was seen as a flattening of the spectra. Furthermore, the total intensity analysis in Lico et al. (2022) showed an epoch when the innermost quasi-stationary feature was seen brightened, and they suggested that K was blended within the stationary feature around this time. In Paper IV, the radio spectra show another flattening around this time in coincidence with the time when the PA in the millimetre bands start to follow the optical data more closely with a 100° difference to the centimetre bands.

These results were used to form a more complete picture of the events taking place in the jet of OJ 287 (see Fig. 9). The time when the moving component K must have resided within the millimetre core coincides with the time when the fast optical PA rotation is seen. These events are also nearly simultaneous with the optical double-flare observed in December 2015 (Valtonen et al. 2016), following the predictions of the binary SMBH impact model (Valtonen et al. 2011). This suggests a possible link between these events. The fast rotations in the optical band could be a result of K travelling down the helical jet magnetic field. In these regions,

the millimetre- and centimetre-radio bands are still optically thick, reflecting only the propagation of the component down the bent jet as suggested by Myserlis et al. (2018). Thus, the fast rotation is only seen in the optical band and as a spectral flattening in the millimetre band. Around the time when the innermost quasi-stationary feature is seen brightened in the VLBI images of Lico et al. (2022), the passage is seen in the radio spectra as a flattening. This is also the time when the PA in the millimetre bands begins to follow the optical PA, signifying that they are optically thin to these jet regions. Lico et al. (2022) also linked the VHE gamma-ray flare observed from OJ 287 with the passage of K through the quasi-stationary feature. With the new revised speed, the timing between the VHE flare and the passage was found to match better, making this scenario more likely. Finally, when K has travelled down the jet bend, the PAs in all bands stabilise.

References

Abdo, A. A., Ackermann, M., Agudo, I., et al. 2010a, ApJ, 716, 30
Abdo, A. A., Ackermann, M., Ajello, M., et al. 2010b, ApJ, 710, 810
Abeysekara, A. U., Benbow, W., Bird, R., et al. 2018, ApJ, 856, 95
Acciari, V. A., Aliu, E., Arlen, T., et al. 2011, ApJ, 738, 25
Acciari, V. A., Aniello, T., Ansoldi, S., et al. 2022, ApJ, 927, 197
Acciari, V. A., Ansoldi, S., Antonelli, L. A., et al. 2019, MNRAS, 486, 4233
Acciari, V. A., Ansoldi, S., Antonelli, L. A., et al. 2020, ApJS, 248, 29
Acharyya, A., Adams, C. B., Archer, A., et al. 2024, ApJ, 973, 134
Achterberg, A., Gallant, Y. A., Kirk, J. G., & Guthmann, A. W. 2001, MNRAS, 328, 393
Ackermann, M., Ajello, M., Albert, A., et al. 2015, ApJ, 813, L41
Agudo, I., Marscher, A. P., Jorstad, S. G., et al. 2012, ApJ, 747, 63
Aharonian, F., Akhperjanian, A. G., Bazer-Bachi, A. R., et al. 2007, ApJ, 664, L71
Aharonian, F. A. 2000, New A, 5, 377
Albert, J., Aliu, E., Anderhub, H., et al. 2007, APJ, 669, 862
Aleksić, J., Ansoldi, S., Antonelli, L. A., et al. 2014a, A&A, 567, A135
Aleksić, J., Ansoldi, S., Antonelli, L. A., et al. 2015, A&A, 578, A22
Aleksić, J., Ansoldi, S., Antonelli, L. A., et al. 2014b, A&A, 569, A46
Aleksić, J., Ansoldi, S., Antonelli, L. A., et al. 2014c, Science, 346, 1080
Aleksić, J., Antonelli, L. A., Antoranz, P., et al. 2011, ApJ, 730, L8
Aliu, E., Archambault, S., Arlen, T., et al. 2014, ApJ, 797, 89
Aller, M. F., Hughes, P. A., Aller, H. D., Latimer, G. E., & Hovatta, T. 2014, ApJ, 791, 53
Angel, J. R. P., Boroson, T. A., Adams, M. T., et al. 1978, in BL Lac Objects, ed. A. M. Wolfe, 117–146
Angelakis, E., Hovatta, T., Blinov, D., et al. 2016, MNRAS, 463, 3365
Ansoldi, S., Antonelli, L. A., Arcaro, C., et al. 2018, ApJ, 863, L10
Arlen, T., Aune, T., Beilicke, M., et al. 2013, ApJ, 762, 92
Asada, K., Inoue, M., Uchida, Y., et al. 2002, PASJ, 54, L39
Asada, K. & Nakamura, M. 2012, ApJ, 745, L28
Axford, W. I., Leer, E., & Skadron, G. 1977, in International Cosmic Ray Conference, Vol. 11, International Cosmic Ray Conference, 132
Barkov, M. V., Aharonian, F. A., Bogovalov, S. V., Kelner, S. R., & Khangulyan, D. 2012, ApJ, 749, 119
Barniol Duran, R., Tchekhovskoy, A., & Giannios, D. 2017, MNRAS, 469, 4957
Baum, S. A., Zirbel, E. L., & O'Dea, C. P. 1995, ApJ, 451, 88
Beckert, T. & Falcke, H. 2002, A&A, 388, 1106
Bell, A. R. 1978, MNRAS, 182, 443
Beskin, V. S. & Nokhrina, E. E. 2006, MNRAS, 367, 375
Bhattacharjee, A., Huang, Y.-M., Yang, H., & Rogers, B. 2009, Physics of Plasmas, 16, 112102
Biretta, J. A., Junor, W., & Livio, M. 2002, New A Rev., 46, 239
Biretta, J. A., Sparks, W. B., & Macchetto, F. 1999, ApJ, 520, 621
Bjornsson, C. I. 1982, ApJ, 260, 855
Blandford, R., Meier, D., & Readhead, A. 2019, ARA&A, 57, 467
Blandford, R., Yuan, Y., Hoshino, M., & Sironi, L. 2017, Space Sci. Rev., 207, 291

Blandford, R. D. & Ostriker, J. P. 1978, ApJ, 221, L29
Blandford, R. D. & Payne, D. G. 1982, MNRAS, 199, 883
Blandford, R. D. & Rees, M. J. 1978, in BL Lac Objects, ed. A. M. Wolfe, 328–341
Blandford, R. D. & Znajek, R. L. 1977, MNRAS, 179, 433
Blinov, D., Jorstad, S. G., Larionov, V. M., et al. 2021, MNRAS, 505, 4616
Blinov, D., Pavlidou, V., Papadakis, I., et al. 2018, MNRAS, 474, 1296
Blinov, D., Pavlidou, V., Papadakis, I., et al. 2016, MNRAS, 462, 1775
Blinov, D., Pavlidou, V., Papadakis, I., et al. 2015, MNRAS, 453, 1669
Bloom, S. D. & Marscher, A. P. 1996, ApJ, 461, 657
Boccardi, B., Migliori, G., Grandi, P., et al. 2019, A&A, 627, A89
Bonnoli, G., Tavecchio, F., Ghisellini, G., & Sbarrato, T. 2015, MNRAS, 451, 611
Böttcher, M. & Els, P. 2016, ApJ, 821, 102
Böttcher, M., Harris, D. E., & Krawczynski, H. 2012a, Relativistic Jets from Active Galactic Nuclei (Wiley-VCH Verlag GmbH & Co. KGaA), 25–27
Böttcher, M., Harris, D. E., & Krawczynski, H. 2012b, Relativistic Jets from Active Galactic Nuclei (Wiley-VCH Verlag GmbH & Co. KGaA), 37–38
Böttcher, M., Harris, D. E., & Krawczynski, H. 2012c, Relativistic Jets from Active Galactic Nuclei (Wiley-VCH Verlag GmbH & Co. KGaA), 32
Böttcher, M., Harvey, J., Joshi, M., et al. 2005, ApJ, 631, 169
Böttcher, M., Reimer, A., Sweeney, K., & Prakash, A. 2013, ApJ, 768, 54
Bresci, V., Lemoine, M., & Gremillet, L. 2023, Physical Review Research, 5, 023194
Britzen, S., Fendt, C., Witzel, G., et al. 2018, MNRAS, 478, 3199
Britzen, S., Zajaček, M., Gopal-Krishna, et al. 2023, ApJ, 951, 106
Celotti, A. & Ghisellini, G. 2008, MNRAS, 385, 283
Cerruti, M., Benbow, W., Chen, X., et al. 2017, A&A, 606, A68
Cerruti, M., Zech, A., Boisson, C., et al. 2019, MNRAS, 483, L12
Chernoglazov, A., Hakobyan, H., & Philippov, A. 2023, ApJ, 959, 122
Cheung, C. C., Harris, D. E., & Stawarz, Ł. 2007, ApJ, 663, L65
Chiaberge, M., Capetti, A., & Celotti, A. 1999, A&A, 349, 77
Christie, I. M., Petropoulou, M., Sironi, L., & Giannios, D. 2019, MNRAS, 482, 65
Christie, I. M., Petropoulou, M., Sironi, L., & Giannios, D. 2020, MNRAS, 492, 549
Cohen, M. H., Meier, D. L., Arshakian, T. G., et al. 2014, ApJ, 787, 151
Cohen, M. H. & Savolainen, T. 2020, A&A, 636, A79
Comisso, L. & Sironi, L. 2018, Phys. Rev. Lett., 121, 255101
Comisso, L. & Sironi, L. 2019, ApJ, 886, 122
Curtis, H. D. 1918, Publications of Lick Observatory, 13, 9
Daly, R. A. & Marscher, A. P. 1988, ApJ, 334, 539
Davis, S. W. & Tchekhovskoy, A. 2020, ARA&A, 58, 407
de Gouveia Dal Pino, E. M. & Kowal, G. 2015, in Astrophysics and Space Science Library, Vol. 407, Magnetic Fields in Diffuse Media, ed. A. Lazarian, E. M. de Gouveia Dal Pino, & C. Melioli, 373
De Young, D. S. 1993, ApJ, 405, L13
del Valle, M. V., de Gouveia Dal Pino, E. M., & Kowal, G. 2016, MNRAS, 463, 4331
Demidem, C., Nättilä, J., & Veledina, A. 2023, ApJ, 947, L10
Dermer, C. D., Murase, K., & Inoue, Y. 2014, Journal of High Energy Astrophysics, 3, 29
Dey, L., Valtonen, M. J., Gopakumar, A., et al. 2021, MNRAS, 503, 4400
Di Gesu, L., Donnarumma, I., Tavecchio, F., et al. 2022, ApJ, 938, L7
Edelson, R. A. & Krolik, J. H. 1988, ApJ, 333, 646
Event Horizon Telescope Collaboration, Akiyama, K., Alberdi, A., et al. 2022, ApJ, 930, L12
Event Horizon Telescope Collaboration, Akiyama, K., Alberdi, A., et al. 2019, ApJ, 875, L1
Fanaroff, B. L. & Riley, J. M. 1974, MNRAS, 167, 31P
Fang, K. & Murase, K. 2018, Nature Physics, 14, 396

Fermo, R. L., Drake, J. F., Swisdak, M. M., Hwang, K., & Wang, Y. 2010, in AGU Fall Meeting Abstracts, Vol. 2010, SM31B–1870
Fossati, G., Maraschi, L., Celotti, A., Comastri, A., & Ghisellini, G. 1998, MNRAS, 299, 433
Gaidos, J. A., Akerlof, C. W., Biller, S., et al. 1996, Nature, 383, 319
Ghisellini, G. 1999, Astrophysical Letters and Communications, 39, 17
Ghisellini, G., Maraschi, L., & Tavecchio, F. 2009a, MNRAS, 396, L105
Ghisellini, G. & Tavecchio, F. 2008, MNRAS, 386, L28
Ghisellini, G., Tavecchio, F., & Chiaberge, M. 2005, A&A, 432, 401
Ghisellini, G., Tavecchio, F., Foschini, L., & Ghirlanda, G. 2011, MNRAS, 414, 2674
Ghisellini, G., Tavecchio, F., Foschini, L., et al. 2010, MNRAS, 402, 497
Ghisellini, G., Tavecchio, F., & Ghirlanda, G. 2009b, MNRAS, 399, 2041
Ghisellini, G., Tavecchio, F., Maraschi, L., Celotti, A., & Sbarrato, T. 2014, Nature, 515, 376
Giannios, D. 2013, MNRAS, 431, 355
Giannios, D., Mimica, P., & Aloy, M. A. 2008, A&A, 478, 747
Giannios, D. & Spruit, H. 2006, in American Institute of Physics Conference Series, Vol. 848, Recent Advances in Astronomy and Astrophysics, ed. N. Solomos (AIP), 530–539
Giannios, D. & Uzdensky, D. A. 2019, MNRAS, 484, 1378
Giannios, D., Uzdensky, D. A., & Begelman, M. C. 2009, MNRAS, 395, L29
Gill, R., Granot, J., & Lyubarsky, Y. 2018, MNRAS, 474, 3535
Giommi, P., Ghisellini, G., Padovani, P., & Tagliaferri, G. 2001, in American Institute of Physics Conference Series, Vol. 599, X-ray Astronomy: Stellar Endpoints, AGN, and the Diffuse X-ray Background, ed. N. E. White, G. Malaguti, & G. G. C. Palumbo (AIP), 441–444
Giommi, P., Glauch, T., Padovani, P., et al. 2020, MNRAS, 497, 865
Giommi, P., Padovani, P., & Polenta, G. 2013, MNRAS, 431, 1914
Giovannini, G., Savolainen, T., Orienti, M., et al. 2018, Nature Astronomy, 2, 472
Giroletti, M., Giovannini, G., Feretti, L., et al. 2004, ApJ, 600, 127
Gómez, J. L., Lobanov, A. P., Bruni, G., et al. 2016, ApJ, 817, 96
Gómez, J. L., Marti, J. M. A., Marscher, A. P., Ibanez, J. M. A., & Marcaide, J. M. 1995, ApJ, 449, L19
Graff, P. B., Georganopoulos, M., Perlman, E. S., & Kazanas, D. 2008, APJ, 689, 68
Güijosa, A. & Daly, R. A. 1996, ApJ, 461, 600
Guo, A., Lu, Q., Lu, S., Wang, S., & Wang, R. 2023, ApJ, 955, 14
Guo, F., Li, X., Daughton, W., et al. 2019, ApJ, 879, L23
Hagen-Thorn, V. A. 1980, Ap&SS, 73, 263
Hardcastle, M. J. & Croston, J. H. 2020, New A Rev., 88, 101539
Hillas, A. M. 1984, ARA&A, 22, 425
Homan, D. C., Cohen, M. H., Hovatta, T., et al. 2021, ApJ, 923, 67
Homan, D. C., Kovalev, Y. Y., Lister, M. L., et al. 2006, ApJ, 642, L115
Homan, D. C. & Lister, M. L. 2006, AJ, 131, 1262
Homan, D. C., Lister, M. L., Kovalev, Y. Y., et al. 2015, ApJ, 798, 134
Homan, D. C. & Wardle, J. F. C. 2004, ApJ, 602, L13
Hovatta, T., Lehto, H. J., & Tornikoski, M. 2008, A&A, 488, 897
Hovatta, T., Leitch, E. M., Homan, D. C., et al. 2013, in European Physical Journal Web of Conferences, Vol. 61, European Physical Journal Web of Conferences (EDP), 06005
Hovatta, T., Lindfors, E., Blinov, D., et al. 2016, A&A, 596, A78
Hovatta, T., Lindfors, E., Kiehlmann, S., et al. 2021, A&A, 650, A83
Hovatta, T., Lister, M. L., Aller, M. F., et al. 2012, AJ, 144, 105
Hovatta, T., Valtaoja, E., Tornikoski, M., & Lähteenmäki, A. 2009, A&A, 494, 527
Huang, Y.-M. & Bhattacharjee, A. 2012, Phys. Rev. Lett., 109, 265002 Hufnagel,
B. R. & Bregman, J. N. 1992, ApJ, 386, 473
Hughes, P. A., Aller, H. D., & Aller, M. F. 1985, ApJ, 298, 301
Hughes, P. A., Aller, H. D., & Aller, M. F. 1989a, ApJ, 341, 54
Hughes, P. A., Aller, H. D., & Aller, M. F. 1989b, ApJ, 341, 68
Hutsemékers, D., Borguet, B., Sluse, D., Cabanac, R., & Lamy, H. 2010, A&A, 520, L7

IceCube Collaboration, Aartsen, M. G., Ackermann, M., et al. 2018, Science, 361, 147
IceCube Collaboration, Abbasi, R., Ackermann, M., et al. 2022, Science, 378, 538
Jannuzi, B. T., Smith, P. S., & Elston, R. 1994, ApJ, 428, 130
Järvelä, E., Lähteenmäki, A., & Berton, M. 2018, A&A, 619, A69
Jogee, S. 2006, in Physics of Active Galactic Nuclei at all Scales, ed. D. Alloin, Vol. 693 (Springer), 143
Jormanainen, J., Hovatta, T., Lindfors, E., et al. 2021, in Proc. 37th Int. Cosm. Ray Conf. — PoS(ICRC2021) (Trieste, Italy: Sissa Medialab), 867
Jorstad, S. & Marscher, A. 2016, Galaxies, 4
Jorstad, S. G., Marscher, A. P., Lister, M. L., et al. 2005, AJ, 130, 1418
Joshi, M. & Böttcher, M. 2007, APJ, 662, 884
Junor, W., Biretta, J. A., & Livio, M. 1999, Nature, 401, 891
Kadler, M., Ros, E., Lobanov, A. P., Falcke, H., & Zensus, J. A. 2004, A&A, 426, 481
Kadowaki, L. H. S., de Gouveia Dal Pino, E. M., Medina-Torrejón, T. E., Mizuno, Y., & Kushwaha, P. 2021, ApJ, 912, 109
Kagan, D., Sironi, L., Cerutti, B., & Giannios, D. 2015, Space Sci. Rev., 191, 545
Kameno, S. 2023, in ALMA at 10 years: Past, Present, and Future, 38
Kankkunen, S., Tornikoski, M., & Hovatta, T. 2025a, A&A, 693, A319
Kankkunen, S., Tornikoski, M., Hovatta, T., & Lähteenmäki, A. 2025b, A&A, 693, A318
Kardashev, N. S., Khartov, V. V., Abramov, V. V., et al. 2013, Astronomy Reports, 57, 153
Kellermann, K. I., Condon, J. J., Kimball, A. E., Perley, R. A., & Ivezić, Ž. 2016, ApJ, 831, 168
Kennel, C. F. & Coroniti, F. V. 1984, ApJ, 283, 710
Kharb, P., Lister, M. L., & Cooper, N. J. 2010, ApJ, 710, 764
Kiehlmann, S., Blinov, D., Liodakis, I., et al. 2021, MNRAS, 507, 225
Kilpua, E. & Koskinen, H. 2017, Introduction to Plasma Physics, 1st edn. (Finland: LIMES)
Kim, J. Y., Krichbaum, T. P., Lu, R. S., et al. 2018, A&A, 616, A188
Kirk, J. G., Rieger, F. M., & Mastichiadis, A. 1998, A&A, 333, 452
Komissarov, S. S. 2001, MNRAS, 326, L41
Komissarov, S. S., Barkov, M. V., Vlahakis, N., & Königl, A. 2007, MNRAS, 380, 51
Komissarov, S. S., Vlahakis, N., Königl, A., & Barkov, M. V. 2009, MNRAS, 394, 1182
Kotilainen, J. K., Falomo, R., & Scarpa, R. 1998, A&A, 332, 503
Kouch, P. M., Lindfors, E., Hovatta, T., et al. 2024, A&A, 690, A111
Kovalev, Y. Y., Lister, M. L., Homan, D. C., & Kellermann, K. I. 2007, ApJ, 668, L27
Kovalev, Y. Y., Pushkarev, A. B., Nokhrina, E. E., et al. 2020, MNRAS, 495, 3576
Kowal, G., de Gouveia Dal Pino, E. M., & Lazarian, A. 2011, ApJ, 735, 102
Krauß, F., Wilms, J., Kadler, M., et al. 2016, A&A, 591, A130
Krymskii, G. F. 1977, Soviet Physics Doklady, 22, 327
Lähteenmäki, A., Järvelä, E., Hovatta, T., et al. 2017, A&A, 603, A100
Lähteenmäki, A. & Valtaoja, E. 1999, ApJ, 521, 493
Lähteenmäki, A., Valtaoja, E., & Wiik, K. 1999, ApJ, 511, 112
Laing, R. A., Jenkins, C. R., Wall, J. V., & Unger, S. W. 1994, in Astronomical Society of the Pacific Conference Series, Vol. 54, The Physics of Active Galaxies, ed. G. V. Bicknell, M. A. Dopita, & P. J. Quinn, 201
Landt, H. & Bignall, H. E. 2008, MNRAS, 391, 967
Li, Z.-Y., Chiueh, T., & Begelman, M. C. 1992, ApJ, 394, 459
Lico, R., Casadio, C., Jorstad, S. G., et al. 2022, A&A, 658, L10
Lindfors, E. J., Hovatta, T., Nilsson, K., et al. 2016, A&A, 593, A98
Lindfors, E. J., Türler, M., Valtaoja, E., et al. 2006, A&A, 456, 895
Liodakis, I., Blinov, D., Potter, S. B., & Rieger, F. M. 2022, MNRAS, 509, L21
Liodakis, I., Peirson, A. L., & Romani, R. W. 2019, ApJ, 880, 29
Liodakis, I., Shablovinskaya, E., Blinov, D., et al. 2023, A&A, 680, L11
Liska, M., Hesp, C., Tchekhovskoy, A., et al. 2018, MNRAS, 474, L81

Lister, M. L., Aller, M. F., Aller, H. D., et al. 2013, AJ, 146, 120
Lister, M. L., Aller, M. F., Aller, H. D., et al. 2016, AJ, 152, 12
Lister, M. L., Homan, D. C., Hovatta, T., et al. 2019, ApJ, 874, 43
Longair, M. S. 1994, High energy astrophysics. Vol.2: Stars, the galaxy and the interstellar medium, Vol. 2 (Cambridge University Press), 351–357
Loureiro, N. F., Samtaney, R., Schekochihin, A. A., & Uzdensky, D. A. 2012, Physics of Plasmas, 19, 042303
Loureiro, N. F., Schekochihin, A. A., & Cowley, S. C. 2007, Physics of Plasmas, 14, 100703
Lucchini, M., Markoff, S., Crumley, P., Krauß, F., & Connors, R. M. T. 2019, MNRAS, 482, 4798
Lynden-Bell, D. 1969, Nature, 223, 690
Lyubarsky, Y. 2009, ApJ, 698, 1570
Lyubarsky, Y. E. 2010, MNRAS, 402, 353
Lyutikov, M. & Lister, M. 2010, ApJ, 722, 197
MAGIC Collaboration, Acciari, V. A., Ansoldi, S., et al. 2020a, A&A, 638, A14
MAGIC Collaboration, Acciari, V. A., Ansoldi, S., et al. 2020b, A&A, 640, A132
MAGIC Collaboration, Ahnen, M. L., Ansoldi, S., et al. 2018, A&A, 619, A45
Mannheim, K. 1993, A&A, 269, 67
Mannheim, K. 1996, Space Sci. Rev., 75, 331
Maraschi, L., Ghisellini, G., & Celotti, A. 1992, ApJ, 397, L5
Marscher, A. P. 2005, Mem. Soc. Astron. Italiana, 76, 168
Marscher, A. P., Di Gesu, L., Jorstad, S. G., et al. 2024, Galaxies, 12, 50
Marscher, A. P. & Gear, W. K. 1985, APJ, 298, 114
Marscher, A. P., Jorstad, S. G., D'Arcangelo, F. D., et al. 2008, Nature, 452, 966
Marscher, A. P., Jorstad, S. G., Larionov, V. M., et al. 2010, ApJ, 710, L126
Mastichiadis, A. & Kirk, J. G. 1995, A&A, 295, 613
Matthews, J. H., Bell, A. R., & Blundell, K. M. 2020, New A Rev., 89, 101543
Max-Moerbeck, W., Hovatta, T., Richards, J. L., et al. 2014, MNRAS, 445, 428
Medina-Torrejón, T. E., de Gouveia Dal Pino, E. M., Kadowaki, L. H. S., et al. 2021, ApJ, 908, 193
Medina-Torrejón, T. E., de Gouveia Dal Pino, E. M., & Kowal, G. 2023, ApJ, 952, 168
Meyer, E. T., Fossati, G., Georganopoulos, M., & Lister, M. L. 2011, ApJ, 740, 98
Meyer, E. T. & Georganopoulos, M. 2014, ApJ, 780, L27
Meyer, E. T., Sparks, W. B., Biretta, J. A., et al. 2013, ApJ, 774, L21
Meyer, E. T., Sparks, W. B., Georganopoulos, M., et al. 2016, ApJ, 818, 195
Mizuno, Y., Gómez, J. L., Nishikawa, K.-I., et al. 2015, ApJ, 809, 38
Morozova, D. A., Larionov, V. M., Troitsky, I. S., et al. 2014, AJ, 148, 42
Mücke, A. & Protheroe, R. J. 2001, Astroparticle Physics, 15, 121
Murase, K., Inoue, Y., & Dermer, C. D. 2014, Phys. Rev. D, 90, 023007
Myserlis, I., Komossa, S., Angelakis, E., et al. 2018, A&A, 619, A88
Nagai, H., Haga, T., Giovannini, G., et al. 2014, ApJ, 785, 53
Nakamura, M., Asada, K., Hada, K., et al. 2018, ApJ, 868, 146
Narayan, R., Kumar, P., & Tchekhovskoy, A. 2011, MNRAS, 416, 2193
Narayan, R. & Piran, T. 2012, MNRAS, 420, 604
Nättilä, J. & Beloborodov, A. M. 2021, ApJ, 921, 87
Netzer, H. 2015, ARA&A, 53, 365
Ni, L., Kliem, B., Lin, J., & Wu, N. 2015, ApJ, 799, 79
Nilsson, K., Pursimo, T., Heidt, J., et al. 2003, A&A, 400, 95
Nilsson, K., Takalo, L., & Piironen, J. 2009, Havaitseva tähtitiede (Tähtitieteellinen yhdistys Ursa), 32–33
Norman, C. A., Melrose, D. B., & Achterberg, A. 1995, ApJ, 454, 60
Oikonomou, F., Murase, K., Padovani, P., Resconi, E., & Mészáros, P. 2019, MNRAS, 489, 4347
Otero-Santos, J., Acosta-Pulido, J. A., Becerra González, J., et al. 2020, MNRAS, 492, 5524

Owen, F. N. & Ledlow, M. J. 1994, in Astronomical Society of the Pacific Conference Series, Vol. 54, The Physics of Active Galaxies, ed. G. V. Bicknell, M. A. Dopita, & P. J. Quinn, 319
Pavlidou, V., Angelakis, E., Myserlis, I., et al. 2014, MNRAS, 442, 1693
Peterson, B. M. 2014, Space Sci. Rev., 183, 253
Petropoulou, M., Giannios, D., & Sironi, L. 2016, MNRAS, 462, 3325
Piner, B. G. & Edwards, P. G. 2004, ApJ, 600, 115
Piner, B. G. & Edwards, P. G. 2018, ApJ, 853, 68
Piner, B. G., Pant, N., & Edwards, P. G. 2008, ApJ, 678, 64
Piner, B. G., Pant, N., Edwards, P. G., & Wiik, K. 2009, ApJ, 690, L31
Plavin, A., Kovalev, Y. Y., Kovalev, Y. A., & Troitsky, S. 2020, ApJ, 894, 101
Pushkarev, A. B., Hovatta, T., Kovalev, Y. Y., et al. 2012, A&A, 545, A113
Pushkarev, A. B., Kovalev, Y. Y., Lister, M. L., & Savolainen, T. 2017, MNRAS, 468, 4992
Raiteri, C. M., Villata, M., Carnerero, M. I., et al. 2023, MNRAS, 526, 4502
Readhead, A. C. S. 1994, ApJ, 426, 51
Rees, M. J. 1966, Nature, 211, 468
Rees, M. J. 1967, MNRAS, 137, 429
Richards, J. L., Max-Moerbeck, W., Pavlidou, V., et al. 2011, ApJS, 194, 29
Rodrigues, X., Fedynitch, A., Gao, S., Boncioli, D., & Winter, W. 2018, ApJ, 854, 54
Salpeter, E. E. 1964, ApJ, 140, 796
Sarkar, A., Gupta, A. C., Chitnis, V. R., & Wiita, P. J. 2021, MNRAS, 501, 50
Savolainen, T., Giovannini, G., Kovalev, Y. Y., et al. 2023, A&A, 676, A114
Savolainen, T., Wiik, K., Valtaoja, E., & Tornikoski, M. 2008, in The role of VLBI in the Golden Age for Radio Astronomy, Vol. 9, 9
Scargle, J. D. 1998, ApJ, 504, 405
Scargle, J. D., Norris, J. P., Jackson, B., & Chiang, J. 2013, ApJ, 764, 167
Scarpa, R. & Falomo, R. 1997, A&A, 325, 109
Sillanpää, A., Haarala, S., Valtonen, M. J., Sundelius, B., & Byrd, G. G. 1988, ApJ, 325, 628
Sillanpää, A., Takalo, L. O., Pursimo, T., et al. 1996, A&A, 305, L17
Sironi, L., Giannios, D., & Petropoulou, M. 2016, MNRAS, 462, 48
Sironi, L., Petropoulou, M., & Giannios, D. 2015, MNRAS, 450, 183
Sironi, L. & Spitkovsky, A. 2014, ApJ, 783, L21
Smith, P. S. 2017, The Astronomer's Telegram, 11047, 1
Smith, P. S., Montiel, E., Rightley, S., et al. 2009, arXiv e-prints, arXiv:0912.3621
Spada, M., Ghisellini, G., Lazzati, D., & Celotti, A. 2001, MNRAS, 325, 1559
Spitkovsky, A. 2008, ApJ, 682, L5
Spruit, H. C., Daigne, F., & Drenkhahn, G. 2001, A&A, 369, 694
Summerlin, E. J. & Baring, M. G. 2012, ApJ, 745, 63
Suray, A. & Troitsky, S. 2024, MNRAS, 527, L26
Takalo, L. O., Nilsson, K., Lindfors, E., et al. 2008, in American Institute of Physics Conference Series, Vol. 1085, American Institute of Physics Conference Series, ed. F. A. Aharonian, W. Hofmann, & F. Rieger, 705–707
Takamoto, M. 2013, ApJ, 775, 50
Tavecchio, F. & Ghisellini, G. 2016, MNRAS, 456, 2374
Tavecchio, F., Maraschi, L., & Ghisellini, G. 1998, ApJ, 509, 608
Tchekhovskoy, A. & Bromberg, O. 2016, MNRAS, 461, L46
Tchekhovskoy, A., McKinney, J. C., & Narayan, R. 2009, ApJ, 699, 1789
Teräsranta, H., Tornikoski, M., Mujunen, A., et al. 1998, A&AS, 132, 305
Tiet, V. C., Piner, B. G., & Edwards, P. G. 2012, arXiv e-prints, arXiv:1205.2399
Tripathi, T., Gupta, A. C., Takey, A., et al. 2024, MNRAS, 527, 5220
Urry, C. M. & Padovani, P. 1995, PASP, 107, 803
Uzdensky, D. A., Loureiro, N. F., & Schekochihin, A. A. 2010, Phys. Rev. Lett., 105, 235002
Valtaoja, E., Lähteenmäki, A., Teräsranta, H., & Lainela, M. 1999, ApJS, 120, 95

Valtaoja, L., Karttunen, H., Valtaoja, E., Shakhovskoy, N. M., & Efimov, Y. S. 1993, A&A, 273, 393
Valtonen, M. J., Lehto, H. J., Nilsson, K., et al. 2008, Nature, 452, 851
Valtonen, M. J., Lehto, H. J., Sillanpää, A., et al. 2006, ApJ, 646, 36
Valtonen, M. J., Mikkola, S., Lehto, H. J., et al. 2011, ApJ, 742, 22
Valtonen, M. J., Zola, S., Ciprini, S., et al. 2016, ApJ, 819, L37
Varglund, I., Järvelä, E., Lähteenmäki, A., et al. 2022, A&A, 668, A91
Vaughan, S., Uttley, P., Markowitz, A. G., et al. 2016, MNRAS, 461, 3145
Vermeulen, R. C., Ogle, P. M., Tran, H. D., et al. 1995, ApJ, 452, L5
Villforth, C., Nilsson, K., Heidt, J., et al. 2010, MNRAS, 402, 2087
Virtanen, J. J. P. & Vainio, R. 2005, ApJ, 621, 313
Vlahakis, N. 2015, in Astrophysics and Space Science Library, Vol. 414, The Formation and Disruption of Black Hole Jets, ed. I. Contopoulos, D. Gabuzda, & N. Kylafis, 177
Wagner, S. J. & Mannheim, K. 2001, in Astronomical Society of the Pacific Conference Series, Vol. 250, Particles and Fields in Radio Galaxies Conference, ed. R. A. Laing & K. M. Blundell, 142
Walker, R. C., Hardee, P. E., Davies, F. B., Ly, C., & Junor, W. 2018, ApJ, 855, 128
Waxman, E. & Bahcall, J. 1998, Phys. Rev. D, 59, 023002
Weisskopf, M. C., Soffitta, P., Ramsey, B. D., & Baldini, L. 2022, in Handbook of X-ray and Gamma-ray Astrophysics, ed. C. Bambi & A. Sangangelo (Springer Living Reference Work), 43
Werner, G. R. & Uzdensky, D. A. 2024, ApJ, 964, L21
Wilson, A. S. & Yang, Y. 2002, ApJ, 568, 133
Zacharias, M., Sitarek, J., Dominis Prester, D., et al. 2017, in International Cosmic Ray Conference, Vol. 301, 35th International Cosmic Ray Conference (ICRC2017), 655
Zavala, R. T. & Taylor, G. B. 2005, ApJ, 626, L73
Zeldovich, J. & Novikov, I. D. 1964, Uspekhi Fizicheskikh Nauk, 84, 377
Zhang, H. 2017, Galaxies, 5, 32
Zhang, H., Li, H., Guo, F., & Taylor, G. 2017, ApJ, 835, 125
Zhang, H., Li, X., Guo, F., & Giannios, D. 2018, ApJ, 862, L25
Zhang, H., Sironi, L., & Giannios, D. 2021, ApJ, 922, 261
Zhang, H., Sironi, L., Giannios, D., & Petropoulou, M. 2023, ApJ, 956, L36
Zhdankin, V., Werner, G. R., Uzdensky, D. A., & Begelman, M. C. 2017, Phys. Rev. Lett., 118, 055103

TURUN
YLIOPISTO
UNIVERSITY
OF TURKU

Painosalama, Turku, Finland 2025

ISBN 978-952-02-0197-5 (PRINT)
ISBN 978-952-02-0198-2 (PDF)
ISSN 0082-7002 (PRINT)
ISSN 2343-3175 (ONLINE)